1   **Short title:** The role of hydrocarbons in cyanobacteria

2   **Corresponding author:** David Lea-Smith.

3   Department of Biochemistry, University of Cambridge, U.K. CB2 1QW

4

5   **Hydrocarbons are essential for optimal cell size, division and growth of cyanobacteria**

6

7   **Authors**: David J. Lea-Smith[1,*], Maite L. Ortiz-Suarez[2], Tchern Lenn[3], Dennis J. Nürnberg[3,†],

8   Laura L. Baers[1], Matthew P. Davey[4], Lucia Parolini[5], Roland G. Huber[6], Charles A. R. Cotton[1,†],

9   Giulia Mastroianni[3], Paolo Bombelli[1], Petra Ungerer[3], Tim J. Stevens[7], Alison G. Smith[4], Peter J.

10   Bond[2,6,8], Conrad W. Mullineaux[3], Christopher J. Howe[1]

11   **Research article**: Membranes, transport and bioenergetics

12   **Affiliations:**

13   [1] Department of Biochemistry, University of Cambridge, Cambridge, CB2 1QW, UK.

14   [2] Centre for Molecular Science Informatics, Department of Chemistry, University of Cambridge,

15   Cambridge, CB2 1EW, UK.

16   [3] School of Biological and Chemical Sciences, Queen Mary University of London, London, E1

17   4NS, UK.

18   [4] Department of Plant Sciences, University of Cambridge, Cambridge, CB2 3EA, UK.

19   [5] Department of Physics, University of Cambridge, Cambridge, CB3 0HE, UK.

20   [6] Bioinformatics Institute, (A*STAR), 30 Biopolis Str., #07-01 Matrix, Singapore 138671.

21   [7] MRC Laboratory of Molecular Biology, Cambridge, CB2 0QH, UK.

1 [8] National University of Singapore, Department of Biological Sciences, 14 Science Drive 4,

2 Singapore 117543.

3

4 **One sentence summary**: Optimal growth and division of cyanobacteria depends upon

5 hydrocarbon induced flexibility in the thylakoid membranes of cyanobacteria, via accumulation

6 of these compounds within the lipid bilayer.

7

8 **Author contributions:** D.J.L-S., C.J.H. conceived the original screening and research plans;

9 D.J.L-S., P.J.B., C.W.M., C.J.H. supervised the experiments; D.J.L-S., M.L.O-S., T.L., D.J.N.,

10 L.L.B., M.P.D., L.P., R.G.H., C.A.R.C., G.M., P.B., P.U. performed most of the experiments;

11 D.J.L-S., M.L.O-S., T.L., D.J.N., L.L.B., M.P.D., R.G.H., T.J.S., P.J.B., C.W.M., C.J.H.

12 designed the experiments and analyzed the data; D.J.L-S., conceived the project and wrote the

13 article with contributions of all the authors; D.J.L-S., P.J.B., C.W.M., C.J.H. supervised and

14 complemented the writing.

15

19

20 † Present address: Department of Life Sciences, Imperial College London, London, SW7 2AZ,

21 UK.

22

1   **Corresponding author e-mail:** djl63@cam.ac.uk

Abstract

Cyanobacteria are intricately organized, incorporating an array of internal thylakoid membranes, the site of photosynthesis, into cells no larger than other bacteria. They also synthesize C15-C19 alkanes and alkenes, which results in substantial production of hydrocarbons in the environment. All sequenced cyanobacteria encode hydrocarbon biosynthesis pathways, suggesting an important, undefined physiological role for these compounds. Here we demonstrate that hydrocarbon deficient mutants of *Synechococcus* sp. PCC 7002 and *Synechocystis* sp. PCC 6803 exhibit significant phenotypic differences from wild type, including enlarged cell size, reduced growth and increased division defects. Photosynthetic rates were similar between strains, although a minor reduction in energy transfer between the soluble light harvesting phycobilisome complex and membrane bound photosystems was observed. Hydrocarbons were shown to accumulate in thylakoid and cytoplasmic membranes. Modelling of membranes suggests these compounds aggregate in the centre of the lipid bilayer, potentially promoting membrane flexibility and facilitating curvature. *In vivo* measurements confirmed that *Synechococcus* sp. PCC 7002 mutants lacking hydrocarbons exhibit reduced thylakoid membrane curvature compared to wild-type. We propose that hydrocarbons may have a role in inducing the flexibility in membranes required for optimal cell division, size and growth, and efficient association of soluble and membrane bound proteins. The recent identification of C15-C17 alkanes and alkenes in microalgal species suggests hydrocarbons may serve a similar function in a broad range of photosynthetic organisms.

Introduction

Cyanobacteria (oxygenic photosynthetic bacteria) are found in nearly every environment on Earth and are major contributors to global carbon and nitrogen fixation (Galloway et al., 2004; Zwirglmaier et al., 2008). They are distinguished amongst prokaryotes in containing multiple internal thylakoid membranes, the site of photosynthesis, and a large protein compartment, the carboxysome, involved in carbon fixation. Despite these extra features, cyanobacteria can be as small as 0.6 µm in diameter (Raven, 1998).

All cyanobacteria with sequenced genomes encode the pathway for the biosynthesis of hydrocarbons, implying an important, although as yet undefined, role for these compounds (Lea-Smith et al., 2015). The major forms are C15-C19 alkanes and alkenes, which can be synthesized from fatty acyl-ACPs by one or other of two separate pathways (Figure 1) (Schirmer et al., 2010; Mendez-Perez et al., 2011). The majority of species produce alkanes and alkenes via acyl-ACP reductase (FAR) and aldehyde deformylating oxygenase (FAD) (Schirmer et al., 2010; Li et al., 2012; Coates et al., 2014; Lea-Smith et al., 2015). Cyanobacterial species lacking the FAR/FAD pathway synthesize alkenes via olefin synthase (Ols) (Mendez-Perez et al., 2011; Coates et al., 2014; Lea-Smith et al., 2015). This suggests that hydrocarbons produced by either pathway serve a similar role in the cell. Homologues of FAR/FAD or Ols are not present in other bacteria, or plant and algal species. However, C15-C17 alkanes and alkenes, synthesized by an alternate, uncharacterized pathway, were recently detected in a range of green microalgae including *Chlamydomonas reinhardtii*, *Chlorella variabilis* NC64A and several *Nannochloropsis* species (Sorigue et al., 2016). In *Chlamydomonas reinhardtii*, hydrocarbons were primarily localized to the chloroplast, which originated in evolution from a cyanobacterium that was engulfed by a host

organism (Howe et al., 2008). Hydrocarbons may therefore have a similar role in cyanobacteria, some green microalgae species and possibly a broader range of photosynthetic organisms.

Hydrocarbons act as antidesiccants, waterproofing agents and signaling molecules in insects (Howard and Blomquist, 2005) and prevent water loss, ensure pollen viability and influence pathogen interactions in plants (Kosma et al., 2009; Bourdenx et al., 2011). However, the function of hydrocarbons in cyanobacteria has not been determined. Characterization of cyanobacterial hydrocarbon biosynthesis pathways has provided the basis for investigating synthetic microbial biofuel systems, which may be a renewable substitute for fossil fuels (Schirmer et al., 2010; Choi and Lee, 2013; Howard et al., 2013). However, secretion of long chain hydrocarbons from the cell into the medium, which is likely essential for commercially viable production, has not been observed in the absence of a membrane solubilization agent (Schirmer et al., 2010; Tan et al., 2011). Cyanobacterial hydrocarbons also have a significant environmental role. Due to the abundance of cyanobacteria in the environment, hydrocarbon production is considerable, with hundreds of millions of tons released into the ocean per annum following cell death (Lea-Smith et al., 2015). This production may be sufficient to sustain populations of hydrocarbon-degrading bacteria, which can then play an important role in consuming anthropogenic oil spills (Lea-Smith et al., 2015).

Here, we investigated the cellular location and role of hydrocarbons in both spherical *Synechocystis* sp. PCC 6803 (*Synechocystis*) and rod-shaped *Synechococcus* sp. PCC 7002 (*Synechococcus*) cells. We developed a model of the cyanobacterial membrane which indicated that hydrocarbons aggregate in the middle of the lipid bilayer and when present at levels

observed in cells, lead to membrane swelling associated with pools of hydrocarbon. This suggested that alkanes may facilitate membrane curvature. *In vivo* measurements of *Synechococcus* thylakoid membrane conformation are consistent with this model.

Results

Hydrocarbons predominantly localize to thylakoid and cytoplasmic membranes

Recently we demonstrated that 115 sequenced cyanobacteria isolated from a broad range of environments contain either the *far/fad* or *ols* genes, encoding the enzymes for alkane/alkene biosynthesis (Lea-Smith et al., 2015). In an additional 32 recently sequenced genomes from cyanobacteria we found the same situation with the majority, 133/147, containing *far/fad* homologues (Table S1). Clearly there is an important role for these compounds in cyanobacteria. In order to investigate this, we disrupted the two different biosynthetic pathways in two species of cyanobacteria that are also morphologically distinct. *Far* in *Synechocystis* and *ols* in *Synechococcus*, were disrupted by insertion of a kanamycin resistance cassette into the open reading frame (Figure S1). In wild-type *Synechocystis* 1.44 mg/g dry cell weight (DCW) of alkanes, predominantly heptadecane and 8-heptadecene were detected (Tan et al., 2011), whereas in *Synechococcus* 0.61 mg/g DCW of alkenes, specifically nonadecene (Mendez-Perez et al., 2011), were present (Figure S2). In contrast, in mutant cells lacking either FAR or Ols, no hydrocarbons were observed. Complementation of ΔFAR by insertion of *far* into a neutral site on the chromosome restored alkanes to wild-type levels (Figure S1; Figure S2).

Due to their hydrophobic and non-polar characteristics, hydrocarbons were expected to localize predominantly to membranes. This was confirmed in purified plasma and thylakoid membrane

fractions from *Synechocystis* (Figure 2A, B). Alkanes constituted 5.63% and 17.41% of the plasma and thylakoid membrane lipid fractions, respectively (Figure 2C; Figure S3). Alkanes comprised 8.92% of the total *Synechocystis* membrane lipid fraction. Given that thylakoids constitute a larger proportion of cellular membrane than plasma membranes this suggests that a hydrocarbon rich portion of the thylakoid membrane was purified during this process. In total *Synechococcus* membrane fractions, alkenes constituted 5.34% of total lipids (Figure 2C).

Hydrocarbon-deficient strains exhibit enlarged cell size and division defects

To determine how loss of hydrocarbons affects cell morphology, we used bright-field microscopy. ΔFAR cells were significantly larger than wild-type *Synechocystis* (11.02 vs 4.63 μm^3) (Figure 3A, B; Figure S4; Table S2), which was confirmed via particle counting measurements (11.49 vs 4.58 μm^3) (Figure 3C; Table S3). In addition, a significantly larger percentage of ΔFAR cells were actively dividing (47.4 vs 40.1%) (Figure 3F; Table S4). Division defects were also apparent in ΔOls, which formed long chains of up to twelve cells and abnormal rods (Figure 3D; Figure S4). The width of ΔOls cells was significantly larger than wild-type *Synechococcus* (1.76 vs 1.61 μm), which resulted in a significant increase in cell volume (3.89 vs 3.08 μm^3) (Figure 3E; Table S2). Overall these results indicate a role for hydrocarbons in limiting cell size and ensuring normal cell division.

Hydrocarbons are essential for optimal cell growth

Strains were then cultured under continuous moderate light (40 μmol photons m^{-2} s^{-1}) to determine whether a lack of hydrocarbons in the membrane affected growth. Due to the difference in cell size between wild-type and hydrocarbon deficient mutants, which affects the

optical properties of the culture (Figure 4A-D), growth was measured both by cell counting and by optical density. The increase in cell number during exponential growth was approximately four fold higher in wild-type *Synechocystis* cultures, compared to ΔFAR (Figure 4A). Moreover, photobleaching increased in ΔFAR cells after two days growth, as measured by the amount of chlorophyll per cell (Figure 4E). This suggests that cell damage was occurring during this time. The enlarged phenotype of ΔFAR was maintained over this growth period (Figure 4G). Wild-type *Synechococcus* also demonstrated a statistically significant 1.4 fold increase in cell number during exponential growth compared to ΔOls (Figure 4B), although photobleaching was not observed (Figure 4F). Under moderate light, when starting with an equal amount of culture as determined by optical density, growth of the wild-type was 2.2 fold faster than ΔFAR (Figure S5A). Growth of wild-type *Synechococcus* was 1.5 fold faster than ΔOls (Figure S5B). The difference in growth rates between wild-type *Synechocystis* and *Synechococcus* and the hydrocarbon deficient mutants was similar at a higher light intensity of 120 µmol photons m^{-2} s^{-1} (Figure S5C, D). Overall these results demonstrate the importance of hydrocarbons for optimal cell growth.

The absence of hydrocarbons has minor effects on photosynthetic performance

Other cellular traits were then examined to determine whether these could affect cell growth. The maximum photosynthetic rate, as measured by oxygen evolution per unit of chlorophyll, was not reduced in the ΔFAR and ΔOls mutants (Figure 5A, B). An increase in respiration was observed in ΔFAR cells, with a two-fold higher rate observed compared to wild-type (Figure 5C). In algae, respiration increases with cellular size (Tang and Peters, 1995), and our data suggest that the same relationship may occur in cyanobacteria. Despite the increased respiratory rate, growth of

ΔFAR was still impaired under light/dark cycles (Figure S6). However, respiration was similar between wild-type and ΔOls (Figure 5D). Photoinhibition was also comparable between wild-type and hydrocarbon deficient strains (Figure 5E, F).

The absorbance profile and emission spectra of the photosynthetic and light harvesting complexes were then examined. Absorbance was slightly reduced in both hydrocarbon deficient mutants in the 400-550 nm range (Figure S7), the portion of the spectra corresponding to carotenoid and chlorophyll absorption. However, the carotenoid/chlorophyll ratio was not significantly different between strains (Table S5), suggesting that the altered absorbance profile of the hydrocarbon-deficient mutants could be due to differences in light scattering, which have a greater effect at shorter wavelengths in the spectrum. Analysis of the hydrocarbon deficient mutants via 77K fluorescence emission spectra showed minor but consistent differences in energy transfer efficiency from phycobilisomes to the reaction centers of photosystems in ΔFAR and ΔOls, a blue shift in the peak between 680-700nm in ΔFAR, indicative of increased uncoupling of phycobilisomes from photosystems (Figure S8A, B), and an altered photosystem II to photosystem I ratio (Figure S8C, D). Given that the oxygen evolution rates of the hydrocarbon deficient strains are similar to wild-type, the cumulative effect of these changes on photosynthetic efficiency must be minor. Overall, these results suggest that differences in cell size and division may be the major factors in the impaired growth observed in hydrocarbon deficient mutants.

Hydrocarbons may induce membrane flexibility by accumulating within the lipid bilayer

Molecular dynamics simulations have become an invaluable technique used to investigate the nanoscale organization of lipid membranes (Marrink et al., 2009; Vattulainen and Rog, 2011), particularly in complex membrane systems (Ingolfsson et al., 2014; Manna et al., 2014). In order to understand how hydrocarbons could affect membrane properties, a novel symmetrical membrane model system was simulated based on the pseudo-atomistic Martini force field, with an approximately 4:1 mapping of heavy atoms to coarse-grained particles (Figure S9) (Lopez et al., 2013). The present model used 16 different lipid types corresponding to the four major groups present in cyanobacteria: phosphatidylglycerol, monogalactosyl-diacylglycerol, digalactosyl-diacylglycerol and sulfoquinovosyl-diacylglycerol, in a ratio as experimentally determined in *Synechocystis* (Table S6) (Sheng et al., 2011). The system contained a total of 2,400 lipids, resulting in a large membrane slab with dimensions of approximately 21 x 27 nm. The hydrocarbon heptadecane was added randomly to the solvent of the equilibrated membranes after 2 μs, and observed to enter the bilayer within the first 50 ps of simulation due to its hydrophobicity. Heptadecane became fully incorporated within ~20 ns, remained solvated within the membrane for the full 5 μs of simulation, and was localized between the two monolayers, alongside the lipid tails at the center of the bilayer (Figure 6A-D).

In symmetrically modeled membranes where no flip-flopping of individual lipids across leaflets occurs, like the one studied here, a flat lamellar bilayer would be expected. This was the case in the absence of alkanes, in which a stable, non-curved membrane was observed (Figure 6A). Addition of hydrocarbons led to their spontaneous insertion and clustering within the bilayer core, with a concomitant increase in membrane thickness from ~3.27 nm to ~3.95 nm, irrespective of concentration. The overall lipid lateral diffusion coefficients in all systems were

within experimentally reported ranges (Kana, 2013). Pools of clustered hydrocarbon molecules were associated with a reduction in lipid chain order and packing efficiency, particularly at ≥5 % mol/mol hydrocarbon concentrations (Figure S10). Moreover, increasing amounts of hydrocarbon dissolved within the bilayer centre which led to localized swelling on one side of the membrane, around the sites of hydrocarbon accumulation, as visually evident in the cross-sections (Figure 6B-D). The swelling settled in one direction or another, and this direction did not change during the simulation, presumably due to the stochastic distribution of solubilized hydrocarbons within the membrane. This is consistent with neutron diffraction studies, which indicated alkane incorporation and swelling of dioleoyl lecithin bilayers (White et al., 1981). The accumulation of hydrocarbons thus increased the flexibility of the membrane and induced localized swelling. It should also be noted that the use of an alternative lipid parameter set developed for the membranes of *Thermosynechococcus vulcanus* and *Spinacia oleracea* (van Eerden et al., 2015) similarly induced swelling and disorder in our bilayer model in the presence of alkanes.

The level of swelling observed at ≥7.5 % mol/mol hydrocarbons due to the presence of a large hydrocarbon pool eventually destabilized the membrane, resulting in a phase transition to a non-lamellar bilayer. In a macroscopic system, and/or under conditions of fixed simulation volume, the membrane swelling and lipid disorder would be expected to result in induction of significant bilayer curvature. Typically, membrane curvature depends upon induced asymmetry of one monolayer compared to another (McMahon and Gallop, 2005). Local clustering of non-bilayer forming lipids could also lead to curvature. Monogalactosyl-diacylglycerol is one such lipid, whereas phosphatidylglycerol, digalactosyl-diacylglycerol and sulfoquinovosyl-diacylglycerol

favor flat lamellar phases (Shipley et al., 1973; Tilcock, 1986), and local monogalactosyl-diacylglycerol enrichment could hinder the formation of complete lamellar bilayer phases, even in combination with other thylakoid lipids (Murphy, 1982).

Synechococcus hydrocarbon-deficient mutants demonstrate reduced membrane curvature

To assess the effects of hydrocarbon deficiency on membrane conformation in _Synechocystis_ and _Synechococcus_ we used thin-section electron microscopy. Electron micrographs of the wild-type and hydrocarbon-deficient mutants suggested that the thylakoid membranes are more planar in the mutants, although this effect could only be properly quantified and verified in _Synechococcus_, due to its more regular thylakoid membrane layout and its elongated cell shape. In thin-section images from _Synechococcus_ we selected cells which appeared circular in profile: in these cases we could be sure that the thin-section cut across the cell perpendicular to the long axis, since any other section would be non-circular (Figure S11). In the circular sections, the thylakoid membranes appear as an array of roughly parallel membrane sacs, each spanning the gap between a pair of poorly-defined bodies close to the plasma membrane termed the "thylakoid centers" (Kunkel, 1982; Stengel et al., 2012). Typically, each thin section showed 2-4 thylakoid centers distributed around the cell perimeter, with the thylakoid membrane sacs extending between them.

To derive a quantitative measure of membrane curvature, we traced the membrane between two thylakoid centers and measured its length, and also measured the straight-line distance between the thylakoid centers (Figure 6E). The ratio of these two measures reflects the curvature of the membrane. We measured the curvature of over 100 membrane segments from each strain. There

was no significant difference between the means of the wild-type and ΔOls inter-node distances. On average, thylakoid membranes in wild-type cells were found to be more curved than those of ΔOls (Figure 6F). The mean length ratio was 1.09 ± 0.06 in wild-type versus 1.06 ± 0.07 in ΔOls, with the relatively high standard deviations reflecting a range of membrane curvatures in both the wild-type and ΔOls (Figure 6F; Figure S12). Nevertheless the difference in the means is highly significant, with a *p*-value of 0.00007 from a Student's *t*-test.

Discussion

Here we have shown a role for hydrocarbons in two morphologically different cyanobacterial species. While both hydrocarbon deficient mutants display increased cell size, division defects and reduced growth, a more severe phenotype was observed in ΔFAR cells (Figure 3; Figure 4). Spherical cells have a larger fraction of highly curved membranes than rod-shaped cells. In the case of cyanobacteria greater membrane flexibility would be required in order to incorporate multiple thylakoid membranes and to divide efficiently. High-resolution inelastic neutron scattering experiments of *Synechocystis* cells demonstrated dynamic flexibility within thylakoid membranes which differed between light and dark periods, suggesting that, if hydrocarbons affect curvature, these compounds may also have a role in other cellular functions (Stingaciu et al., 2016). While the division dynamics of cyanobacteria are poorly understood, in the spherical bacterium *Staphylococcus aureus*, cells divide by first forming a septum, leading to development of two daughter cells connected via a narrow peripheral ring, followed by an abrupt separation event (Zhou et al., 2015). This form of division induces high stress on cellular components and is dependent on extreme curvature in membranes. A similar division event in *Synechocystis* and other spherical cyanobacteria requires the induction of membrane curvature not only in the

cytoplasmic membrane but also in the thylakoid membranes, in order that these are efficiently distributed between daughter cells. By contrast, rod shaped cells divide by first increasing in volume and length, followed by formation of a septum in the middle of the extended cell and subsequent separation (Wu and Errington, 2012). This form of cell division would require less induction of membrane curvature in the cytoplasmic membrane and thylakoid membranes and would be necessary at only one end of the cell. Interestingly, in the ΔOls strain, hydrocarbons were more important for efficient daughter cell separation than division, as shown by the formation of chains of cells (Figure 3D).

Although the ΔOls mutant showed significantly less thylakoid membrane curvature on average than wild-type *Synechococcus*, examples of membrane curvature could be observed in this strain (Figure 6, Figure S11), despite the natural tendency of lipid bilayers to adopt a flat shape (Graham and Kozlov, 2010). Moreover, since simulations indicated that they integrate into the middle of the bilayer (Figure 6B-D), hydrocarbons would be unable to orientate the direction of curvature, suggesting that their major role may be to induce the required flexibility in membranes. Therefore hydrocarbons cannot be the only factor determining membrane curvature: other factors must contribute to both the direction and maintenance of curvature. In addition it was observed that after successive rounds of sub-culturing, typically six to eight, that the size difference between the hydrocarbon deficient mutants and wild-type strains was reduced and *Synechococcus* ΔOls cells no longer formed chains of cells. That suggests that other factors in the cell were compensating for the loss of hydrocarbons.

An *Arabidopsis thaliana* protein, CURT1A, has been shown to induce membrane curvature in chloroplast membranes (Armbruster et al., 2013). A homologous protein in *Synechocystis*, CurT, has recently been shown to have a similar role in thylakoid membranes (Heinz et al., 2016). Deletion of CurT resulted in a reduction in growth and extreme differences in thylakoid membrane organization, with the thylakoids appearing to cross the cytoplasm and not converging on the 'thylakoid centres'. In contrast to ΔFAR, cell size was not affected although photosynthesis was reduced. The Δ*curT* strain also displayed disassociated phycobilisomes, similar to what was observed in ΔFAR and ΔOls (Figure S8A, B). This strongly suggests that the degree of membrane curvature is essential for optimal phycobilisome:photosystem interaction and may also influence contact of other soluble proteins with membrane bound components. Therefore it is possible that, if hydrocarbons do alter membrane curvature, then this is augmented and orientated by CurT. In Δ*curT*, the thylakoid membranes were still highly curved, indicating that other factors are involved in inducing membrane curvature (Heinz et al., 2016). Homologues of CurT are present in the majority of sequenced cyanobacterial strains (Table S1). Notable exceptions include *Gloeobacter* species, which lack thylakoid membranes (Rippka et al., 1974; Rexroth et al., 2011; Saw et al., 2013), and therefore may not require orientation of membrane curvature or may regulate it by other means. In other bacterial species this includes turgor pressure or force applied via cytoskeletal components (Cabeen et al., 2009). The glycolipid monogalactosyl-diacylglycerol may also help stabilize this curvature, given its tendency to favor non-lamellar phases (Shipley et al., 1973; Murphy, 1982; Tilcock, 1986). Other as yet unidentified factors may also contribute to membrane curvature.

Hydrocarbons may also have additional functions in cells not identified in this study, such as modulating membrane permeability (Valentine and Reddy, 2015). The use of planar lipid bilayers as model systems has demonstrated that the addition of hexadecane increases membrane thickness and reduces membrane permeability (Dilger and Benz, 1985). Therefore, the increase in cell size may be due to a combination of factors: differences in osmotic pressure due to reduced membrane permeability; outward physical pressure on the cell applied by a series of less curved thylakoid membranes; and division impairment, which would result in hydrocarbon deficient strains being larger than wild-type before cell separation. However, in the case of *Synechococcus* cells it is interesting that an increase in size was only observed along the long axis of the cell, where outward physical pressure applied by less curved thylakoid membranes would be expected to have the greatest effect.

Conclusion

Given that maintaining optimal growth and cell division is important in all ecosystems (Raven, 1998), the role of hydrocarbons in supporting optimal growth through potentially inducing membrane flexibility and reducing membrane permeability may be sufficient to explain the strong evolutionary pressure to retain hydrocarbon biosynthesis in cyanobacteria. It may also explain why similar hydrocarbons are produced by some microalgae species. An additional advantage is that unlike phospholipids or proteins, hydrocarbons do not contain either phosphorus or nitrogen, which are limited in many environments, notably in the open ocean where *Synechococcus* and *Prochlorococcus* species dominate (Flombaum et al., 2013). Moreover, the non-reactive properties of hydrocarbons make them resistant to oxidative damage (Valentine and Reddy, 2015), which is a major issue in cyanobacteria due to constant electron

production from photosynthesis and respiration (Lea-Smith et al., 2015). Hydrocarbon induced membrane curvature may therefore represent a unique, low-risk and efficient system of inducing flexibility and reducing permeability in one of the most biologically important and ancient membrane systems on the planet.

Materials and methods

Bioinformatics

Protein BLAST comparisons (Altschul et al., 1990) were performed using inferred protein sequences for *Synechocystis sll0209* (FAR), *sll0208* (FAD) and *slr0483* (CurT) and *Synechococcus* Syn7002_A1173 (Ols) (WP_012306795) with the completed cyanobacterial genomes listed in the NCBI database (http://www.ncbi.nlm.nih.gov/genome/browse/) and Biller *et al*, 2014 (Biller et al., 2014). For FASTA BLAST comparisons of Ols only matches across the majority of the gene (>90%) were included, due to the conservation of many domains in polyketide synthase proteins. Protein BLAST comparisons of FAR, FAD and Ols were also performed against the bacterial and eukaryotic sequences in the NCBI database in order to confirm that these proteins are cyanobacterial specific.

Bacterial strains, media and growth conditions

Synechocystis and *Synechococcus* strains were routinely cultured in BG11 medium with 10 mM sodium bicarbonate (Castenholz, 1988) at 30°C and grown under moderate light (30-40 µmol photons m^{-2} s^{-1}) with shaking at 120 rpm unless otherwise indicated. HEPES and vitamin B12 were added to *Synechococcus* cultures to a final concentration of 10 mM and 4 µg/L, respectively. 10 mM sodium bicarbonate was also added to *Synechococcus* cultures every two

days. 15 g/L of agar was used for preparation of solid media and supplemented with 30-100 µg/mL of kanamycin or 5% sucrose (w/v) when necessary. Cultures incubated at 120 µmol photons m^{-2} s^{-1} were bubbled with air to prevent carbon limitation.

Plasmid construction

All primers are listed in Table S7. Polymerase chain reactions were performed by standard procedures using Phusion high fidelity DNA polymerase (NEB). The genome sequence of *Synechocystis* and *Synechococcus* (Kaneko et al., 1996) was consulted via Cyanobase (http://genome.kazusa.or.jp/cyanobase) for primer design. Gene deletion of *Sll0209* was performed by amplifying a 1750 bp fragment spanning *Sll0209* and flanking regions using primers Sll0209for and Sll0209rev, followed by insertion into the *Xba*I/*Sph*I sites of pUC19. The *aph* gene conferring kanamycin resistance was excised from pUC4K (Vieira and Messing, 1982) and inserted into the *Hinc*II site in the middle of the fragment to generate pSll0209. Gene deletion of *ols* (SYNPCC7002_A1173) was performed by amplifying a 1922 bp fragment in the 5' region using primers Olsfor and Olsrev, followed by insertion into the *Eco*RI/*Sal*I sites of pUC19. The *aph* gene was inserted into the blunt ended *Bam*HI in the middle of the fragment to generate pOls.

Gene deletion of *phaAB* was performed by amplifying a 1069 bp fragment upstream of *phaA* using primers PhaABleftfor and PhaABleftrev and a 1087 bp fragment downstream of *phaB* using primers PhaABrightfor and PhaABrightrev, followed by insertion of the respective fragments into the *Xba*I/*Bam*HI and *Sac*I/*Eco*RI sites of pUC19 to generate pPhaAB-1. The *Bam*HI digested *npt1/sacRB* cassette from pUM24Cm (Ried and Collmer, 1987) was inserted

19

into the *Bam*HI site between the upstream and downstream fragments to generate pPhaAB-2. To generate the plasmid for complementation (pSll0209comp) of ΔSll0209 the entire Sll0209 gene plus 295 bp of upstream region and 263 bp of downstream region was amplified using primer pairs Sll0209compfor and Sll0209comprev and inserted into the *Bam*HI/*Sac*I sites of pPhaAB-1.

Generation of mutant strains

Generation of marked mutants was conducted according to Lea-Smith *et al* (Lea-Smith et al., 2013; Lea-Smith et al., 2016). Approximately 1 μg of plasmids pSll0209, pOls and pPhaAB-2 were mixed with *Synechocystis* or *Synechococcus* cells for 6 hours in liquid medium, followed by incubation on BG11 agar plates for approximately 24 hours. An additional 3 mL of agar containing kanamycin was added to the surface of the plate followed by further incubation for approximately 1-2 weeks. Transformants were sub-cultured to allow segregation of mutant alleles. In the case of the hydrocarbon deficient mutants this was performed by streaking the strains on BG11 agar plates containing 30 μg/mL of kanamycin, followed by a subsequent re-streak on a BG11 agar plate containing 100 μg/mL of kanamycin. Typically, segregated mutants were obtained within two weeks. This is in contrast to a recent report, in which hydrocarbon deficient *Synechocystis* mutants were only obtained after approximately six months, most likely due to these strains being segregated on BG11 agar plates containing a maximum of 40 μg/mL of kanamycin (Berla et al., 2015). Repeated streaking over a six month period could also result in selection of numerous secondary mutations. Given that a complemented strain was not generated or examined in the Berla *et al* study it is therefore impossible to determine whether the phenotype observed was caused by deletion of hydrocarbons or secondary mutations. Due to this factor and the difference in time in generating mutants a direct comparison between the results

reported by Berla *et al* (Berla et al., 2015) and this study is difficult due to the instability of the hydrocarbon deficient strains.

Segregation was confirmed by PCR using primers Sll0209for/Sll0209rev, Olsfor/Olsrev or Phafor/Pharev, which flank the inserted region (Figure S1). Generation of unmarked mutants was carried out according to Xu *et al* (Xu et al., 2004) and Lea-Smith *et al* (Lea-Smith et al., 2013; Lea-Smith et al., 2016). To remove the *npt1/sacRB* cassette and insert the Sll0209 complementation cassette, the *phaAB* marked knockout was transformed with 1 μg of the markerless pSll0209comp construct. Following incubation in BG11 liquid medium for 4 days and agar plates containing sucrose for a further 1-2 weeks, transformants were patched on kanamycin and sucrose plates. Sucrose resistant, kanamycin sensitive strains containing the unmarked deletion were confirmed by PCR using primers flanking the insert region (Figure S1B). The ΔSll0209 mutant was generated in the ΔPhaAB:Sll0209 background in order to produce the complement strain.

The ΔOls mutant could not be complemented due to the large size of the gene (8163 bp). Therefore wild-type *Synechococcus* and ΔOls were sequenced using the IlluminaMiSeq personal sequencer and mapped to the *Synechococcus* genome. Apart from the expected deletion in *ols*, only a single point mutation in ΔOls, leading to a silent mutation, was observed, when compared to the wild-type.

For characterization, mutant strains were sub-cultured in liquid medium no more than two times and streaked on solid medium a maximum of six times, due to the instability of the mutants.

After this period the size difference between the hydrocarbon deficient mutants and wild-type strains was reduced, suggesting that another factor in the cell was compensating for the loss of hydrocarbons. Strains could not be prepared as glycerol stocks, since this also resulted in a change in the phenotype. After this period of sub-culturing, fresh mutants were constructed for analysis.

Extraction and analysis of total hydrocarbons

All chemicals were purchased from Sigma chemicals. For extraction of total hydrocarbons, 1.5 mL of dichloromethane was added to pelleted dried cells in glass vials and hydrocarbons were extracted and analyzed by gas chromatography-mass spectrometry (GC-MS) according to Lea-Smith *et al* (Lea-Smith et al., 2015). Hydrocarbons and lipids were extracted from *Synechocystis* thylakoid, cytoplasmic and total membrane fractions and *Synechococcus* total membrane fractions based on the method in Davey *et al* (Davey et al., 2008) where 1 mL (3 mL for total membrane fractions) of chilled (–20 °C) solvent (methanol:chloroform:water, 2.5:1:1) was added to the membrane fraction tube, vortexed, and left in ice with occasional shaking. After 30 min, tubes were centrifuged (16,000 g, 2 min, 4˚C). The supernatant was removed and placed in a chilled tube on ice. The remaining pellet was re-extracted with 0.5 mL (1.5 mL for total membrane fractions) chilled (–20˚C) methanol:chloroform, 1:1 for 30 min. After centrifuging as described earlier, the supernatants were combined in a 2 mL tube. The organic chloroform phase was separated from the aqueous phase by adding 250 μL (750 μL) chilled water and extracted into a new glass 2 mL GC sample vial. The chloroform phase was dried (GeneVac EZ-2; SP Scientific) and re-suspended in 200 μL heptane. The extracts were stored at –80˚C before analysis of total alkanes and lipids (FAMEs). For negative controls, extraction blanks were

carried out without cyanobacteria (no significant amounts of hydrocarbons were detected) and positive controls consisted of adding 1 mg/mL standard alkane mix (Sigma C8-C20 Alkane mix) to a blank extraction procedure.

Purification of membrane fractions

Plasma and thylakoid membranes were isolated using a combination of sucrose density centrifugation followed by aqueous two-phase partitioning according to Norling *et al* (Norling et al., 1998) and Huang *et al* (Huang et al., 2002). *Synechocystis* cells were grown at 30°C under 50 μmol photons m^{-2} s^{-1} of white light in BG-11 medium with bubbling air. All steps were carried out at 4°C unless otherwise stated. 2 L of cells harvested at OD_{750nm} = 0.9-1.0 were resuspended in Buffer A (20mM potassium phosphate pH7.8) and broken with glass beads. Unbroken cells and debris was pelleted by centrifugation at 3,000 x g for 10 min. The supernatant was centrifuged at 103,000 x g for 30 min to pellet total membranes. Total membranes were made up to a concentration of 42% sucrose by the addition of solid sucrose and placed onto a discontinuous sucrose gradient comprising of 3ml layers of 50% (w/w), 42% (w/w with total membranes), 40% (w/w), 38% (w/w), 35% (w/w), 30% (w/w), 10% (w/w) sucrose in Buffer A, and centrifuged at 125,000 x g for 15 hours. The fraction between 38-42% was collected, diluted with Buffer A and centrifuged at 125,000 x g for 45 min to pellet membranes. Pelleted membranes were homogenized in Buffer B (5mM potassium phosphate pH7.8, 0.25M sucrose) to a weight of 3.75 g and applied to a 6.25 g polymer mixture of 5.8% Dextran T-500 and 5.8% polyethylene glycol 3350 in Buffer B. The partitioning system was gently inverted 35 times at 4°C and centrifuged at 1000 x g to facilitate phase separation. Pure thylakoid membranes were obtained from the lower phase after five further partitionings in the 5.8% polymer mixture. Pure

plasma membranes were obtained from the ninth upper phase after three partitionings in the initial polymer mixture of 5.8%, three further partitionings in 6.2% and a final three partitionings in 6.4%. Purified plasma and thylakoid membranes were diluted in Buffer B and pelleted by centrifugation at 125,000 x g for 1 hour and homogenized in a minimal volume of the same buffer.

Identification and quantification of hydrocarbons in the membrane fractions

Hydrocarbons in the heptane extract were identified by GC-MS (Thermo Scientific Trace GC 1310 – ISQ LT Single Quadruple EI MS, A1-1310 Autosampler) with a Phenomenex Zebron ZB-5MSi Capillary GC Column (30m x 0.25mm x 0.25 μm). The injection volume was 1 μL with a 10:1 split ratio with an injector temperature of 300 °C, using helium as a carrier gas at a constant flow of 1.0 mL min^{-1}. The following gradient was used: initial oven temperature 70 °C, 2 min; 76 °C, 1 min; 250 °C at 6 °C min^{-1}; 330 °C at 50 °C min^{-1}. The transfer line temperature was 250 °C. The mass spectrometry conditions in the positive mode were: ion source, 250 ℃; mass range 45-650 Da; scan time of 0.35 seconds. Heptadecane and nonadecene were identified by co-retention with standards and NIST mass spectral search libraries (National Institute of Standards and Technology NIST v2.0), 8-heptadecene was identified using the NIST library alone. Heptadecane and nonadecene were quantified using standard curves derived from peak areas of heptadecane and nonadecene standards, 8-heptadecene was quantified using peak areas derived from heptadecane standards (0.06 - 31 μg/mL).

Identification and quantification of total lipids in the membrane fractions

The total lipid content of the heptane extract was converted to fatty acid methyl esters (FAMEs) as described by Davey *et al* (Davey et al., 2014). The FAMEs were separated and identified using GC-MS as described in the membrane alkane analysis section but with a 35:1 split injection ratio, injector temperature of 230 °C, helium at a constant flow rate of 1.2 ml min^{-1}, and with the following gradient: initial oven temperature, 60 °C for 2 min; 150 °C at 15 °C min^{-1}; 230 °C at 3.4 °C min^{-1}. The detector temperature was 250 °C with a scan time of 0.174 seconds. FAMEs were identified by co-elution with a FAME standards and NIST libraries and were quantified and summed using standard curves derived from C16:0 methyl esters.

Modelling of *Synechocystis* membranes

The *in silico* cyanobacterial membrane lipid compositions were based on the experimental lipid extractions and characterization of *Synechocystis* by Sheng *et al* (Sheng et al., 2011). Four major classes of cyanobacterial lipids were used: phosphatidylglycerol (PG), monogalactosyl-diacylglycerol (MGDG), digalactosyl-diacylglycerol (DGDG) and sulfoquinovosyl-diacylglycerol (SQDG), with various acyl tails differing in length and degree of saturation. These lipids contain a palmitic (16:1$^{\Delta 9}$) tail at the *sn*-2 position, and another acyl tail of variable length and saturation at the *sn*-1 position (Murata et al., 1992). The composition of the lipid tails in the *in silico* membranes was adapted to coarse grained resolution, i.e. an approximately 4:1 mapping of heavy atoms to coarse-grained particles, using the Martini force field (Lopez et al., 2013). The structure of the lipid head groups and representative tails included in the model are compared to their coarse grained topologies in Figure S9, where the mapping of the Martini bead types are shown and labeled. Standard bonded parameters were used. The compositions determined by Sheng *et al* (Sheng et al., 2011) are shown in Table S6, and compared to the number of lipids

used in our model membranes to reproduce as closely as possible this composition. The hydrocarbon heptadecane was added in varying quantities to study the effects of this compound on membrane properties.

A total of 2,400 lipids were used to build symmetric bilayers, consisting of 16 different lipid types. The system was solvated with 11,323 water beads, corresponding to ~45,000 waters, ensuring that the bilayer was well hydrated. Hydrated sodium counterion particles were added to neutralize the charges of PG and SQDG lipids. Heptadecane was added randomly to the solvent in the equilibrated membranes after 2 µs. The amounts used were 2.5, 5.0 and 7.5 mol %, corresponding to 60, 120 and 180 alkane molecules, respectively. The initial unit cell dimensions of all membrane systems were 21.0 x 27.5 x 9.0 nm in the x, y, and z directions.

Simulation details

The molecular dynamics simulations were performed using the GROMACS 4.5.5 MD package. The Martini lipid force field was used (Marrink et al., 2007), due to its proven performance in describing complex lipid membrane properties. Initially, a system containing 200 randomly placed 18:1 DGDG molecules surrounded by solvent was simulated for 200 ns, yielding a pre-equilibrated bilayer. The lipid types were then converted at random to yield a membrane with the appropriate composition (Table S6), using in-house code. Following minimization and a further 200 ns equilibration, the coordinates of this bilayer system were then multiplied in the x- and y-dimensions to produce the full 2,400 lipid bilayer. A 1 µs equilibration simulation followed. Steepest descent was used for minimization, and a 40 fs time step was used together with the leap-frog algorithm during simulations. Lennard-Jones (excluding scaled 1-4) interactions were

smoothly switched off between 0.9 and 1.2 nm, using a force switch. Electrostatic interactions were calculated using a shifted potential with a cut-off of 1.2 nm, with a distance-dependent dielectric constant of 15. The neighbor list of 1.4 nm was updated every 10 steps. The isothermal-isobaric ensemble (NpT) was used. The pressure (1 bar) and temperature (316 K) coupling parameters were set to 5 ps semi-isotropically, and 10 ps, respectively (Berendsen et al., 1984). All systems were simulated for 5 µs.

Electron Microscopy

Synechococcus cultures were grown to OD$_{750nm}$ = ~0.3 and harvested by centrifugation (3000 x g; 10 min), fixed and embedded according to the protocol described in Nürnberg *et al* using potassium permanganate as additional fixative (Nurnberg et al., 2014). Thin sections were cut with a glass knife at a Reichert Ultracut E microtome and collected on uncoated, 300 mesh copper grids. High contrast was obtained by post-staining with saturated aqueous uranyl acetate and lead citrate (Reynolds, 1963) for 4 min each. The grids were examined in a JOEL JEM-1230 transmission electron microscope at an accelerating potential of 80 kV.

Curvature measurements

In transverse sections, the thylakoid membranes, 3-5 membranes thick, of wild-type *Synechococcus* and ΔOls cells, appear to emanate from 3-4 well-spaced nodes on the edge of the cell, like pages of a book, which is lying open, that fan out from its spine. The "spine" of this "book" can be imagined to run longitudinally along the cell from pole to pole. Spline curves were hand-fitted to individual membrane layers as far as they could be traced by eye from node to node in ImageJ. The ratio of the length of the curved line drawn to its Feret diameter

(maximum calliper distance – i.e. the straight line distance between start and end points of the line in most cases) was taken to be a measure of its curvature. The 124 membranes from 9 wild-type cells and 102 membranes form 12 ΔOls cells were analyzed. Statistical tests were performed in Matlab.

Confocal fluorescence Microscopy

For confocal microscopy, mid-logarithmic phase cells were spotted onto BG11 1 % (w/v) agar plates and visualized with a Leica laser-scanning confocal microscope SP5 using a x63 oil-immersion objective (Leica HCX PL APO lambda blue 63.0x1.40 OIL UV). Chlorophyll *a* fluorescence was detected by using an excitation wave length of 488 nm and an emission range from 670 to 720 nm. Images were captured with a pinhole of 95.5 μm which corresponds to an optical section thickness of 0.8 μm and by 4x line averaging. Analyses were performed with ImageJ 1.47i (http://imagej.nih.gov/ij) and Origin. The cell volume was determined from the mean diameter for *Synechocystis* cells assuming a sphere, and from the mean diameter and width of *Synechococcus* cells by assuming an ellipsoidal shape. A Student's *t* test was used for comparison of cell volumes between strains with $P<0.05$ being considered statistically significant.

Cell counting

Numbers of cells per unit of volume were measured by counting the cells directly using a Beckman Coulter 2Z particle counter. Measurements were performed by diluting 20-100 μL of cells in 10 mL of measuring buffer. The cell diameter of *Synechocystis* cells was directly measured using the same instrument. Cell volume was calculated from these measurements. Due

to the rod shape of *Synechococcus*, the cell size of this bacterium could not be determined using this device.

Cell division

A semi-automated counting of cells was used to determine the number of cells that were in the process of division by segmenting the image based on fluorescence intensity and cell size. A frequency table of the number of cells observed to be above and below the size threshold (interpreted to be dividing and divided respectively) was generated (Table S4). A 2-way Chi-square test yielded a significant result showing that the proportions of dividing versus divided cells is not independent of the strain and therefore suggests that there are more dividing cells in ΔFAR than in the wild-type with statistical significance.

Measurements of cell growth

Growth rate constants as determined by cell counting were calculated during early exponential phase (0-46 hours and 0-44 hours, respectively, for *Synechocystis* and *Synechococcus* strains cultured under 40 μmol photons m^{-2} s^{-1} light). Growth rate constants as determined by optical density were calculated during early exponential phase (0-40 hours and 0-90 hours, respectively, for *Synechocystis* strains cultured under 40 and 120 μmol photons m^{-2} s^{-1} light; 0-26 hours and 0-90 hours, respectively, for *Synechococcus* strains cultured under 40 and 120 μmol photons m^{-2} s^{-1} light; and 18-78 hours for *Synechocystis* strains cultured under 12 hour light (40 μmol photons m^{-2} s^{-1})/12 hour dark cycles). A Student's paired *t* test was used for comparison of growth between strains, $P<0.05$ being considered statistically significant.

Chlorophyll measurements

The amount of chlorophyll in *Synechocystis* samples was measured by subtracting the 750 nm optical density (OD) value from the 680 nm OD value and multiplying the total by 10.854, according to Lea-Smith *et al* (Lea-Smith et al., 2013). To determine the correlation between OD values versus the chlorophyll concentration of *Synechococcus*, a range of samples was measured at 750 nm and 680 nm, in addition to measuring the chlorophyll concentration according to the method of Porra *et al* (Porra et al., 1989). A strong correlation ($r^2 = 0.9983$) was observed (Figure S13). The amount of chlorophyll in *Synechococcus* samples was then measured by subtracting the 750 nm OD value from the 680 nm OD value and multiplying the total by 12.959.

Photosynthesis, photoinhibition and respiration measurements

Photoinhibition, photosynthesis and respiration were determined according to Lea-Smith *et al* (Lea-Smith et al., 2014). Photosynthetic O_2 evolution rates and O_2 depletion rates (respiration) were determined on cell cultures at OD_{750nm} = ~0.5 (~2.3 nmol Chl ml^{-1} in *Synechocystis* or ~4 nmol Chl ml^{-1} in *Synechococcus*) using an oxygen electrode system (Hansatech Ltd) maintained at 30°C. ΔFAR cell cultures were collected at an OD_{750nm} = ~0.4 and concentrated to an OD_{750nm} = ~0.5 prior to analysis. Following dark equilibration (10 min), O_2 exchange rates were recorded for 10 min at increasing light intensities (10, 20, 50, 95, 240, 450, 950 and 2000 μmol photons m^{-2} s^{-1}), using Realite MR16+C 24°, 12 volt, 50 watt C13 white LED lamps (Deltech UK, London), which have a spectra similar to sunlight. Each light period was followed immediately by 10 min in darkness to calculate the respiration rates. The respiration rate following illumination at each light intensity period was subtracted to estimate the real rate of photosynthetic O_2 evolution. To measure photoinhibition, cell cultures of OD_{750nm} = ~0.2 (~1

nmol Chl ml^{-1} in *Synechocystis* or ~1.3 nmol Chl ml^{-1} in *Synechococcus*) were first dark equilibrated (10 min), and the rate of O_2 evolution was recorded for 50 min at a light intensity of 2000 µmol photons m^{-2} s^{-1} in *Synechocystis* and 3000 µmol photons m^{-2} s^{-1} in *Synechococcus*. All measurements were standardized to the initial rate. A Student's paired t test was used for all comparisons, $P<0.05$ being considered statistically significant.

77K fluorescence

77K fluorescence measurements were performed on cells harvested during the exponential growth phase at an OD_{750nm} = ~0.3, diluted to a final chlorophyll concentration of 5 µM and placed into glass sample tubes. After dark adaptation at room temperature for approximately 10 min, samples were then snap-frozen in liquid nitrogen. 77K Fluorescence emission spectra were recorded by a Perkin Elmer LS55 fluorescence spectrometer from 620nm − 800nm with either 600 nm (phycobilisome excitation) or 435 nm (chlorophyll excitation).

Absorbance measurements

Absorbance measurements on whole cells were performed according to Lea-Smith *et al* (Lea-Smith et al., 2014). Cultures were harvested during the exponential growth phase at an OD_{750nm} = ~0.4. Cultures were placed in a 4 ml fluorescence cuvette (1 cm path length) and positioned in front of the entrance port of an integrating sphere. A light source sent light via an input fiber into the cuvette containing the sample and the light leaving the sample in the forward direction was collected by the integrating sphere. The extinction spectra were recorded using a USB4000-UV-VIS Ocean Optics Spectrometer connected to the integrating sphere with an output fibre optic and interfaced to a computer. The cuvettes containing the samples were positioned at different

distances (0 mm and 5 mm) from the entrance port of the sphere and the absorbance spectrum was obtained via the SpectraSuite® Spectroscopy operating software. The nominal absorption spectrum was then calculated using the equation according to Merzlyak *et al*, 2000 (Merzlyak and Naqvi, 2000).

Carotenoid quantification

High performance liquid chromatography (HPLC) was performed to analyze carotenoid/chlorophyll *a* ratios. Pigments were extracted from freeze dried samples (triplicates) by three subsequent extraction steps in ice-cold methanol. After addition of methanol the samples were vortexed vigorously, incubated on ice for 10 min and centrifuged for 10 min at 4 °C at 14,000 rpm. The supernatants of all three extraction steps were combined and filtered using 13 mm, 0.22 µm PTFE syringe disc filters. 200 µl of each sample was loaded onto a Dionex HPLC system, which was equipped with a LiChrospher 100 RP-18 (5um) reverse-phase column (Merck 1.50943.0001). The flow rate was set at 1 mL/min and the mobile phase composed of two eluents (A: 0-12 min; B: 12-23 min). A: 87% acetonitrile, 10% methanol, 3% 0.1M Tris buffer pH-8. B: 80% methanol, 20% hexane. Pigments were detected spectrophotometrically at 447 nm and absorbance spectra data was collected from 350-750 nm. The relative quantity of each pigment resolved was determined by integration of the area under the 447 nm peak (mAUxmin). Pigments were identified using published absorbance spectra data (Mohamed and Vermaas, 2004).
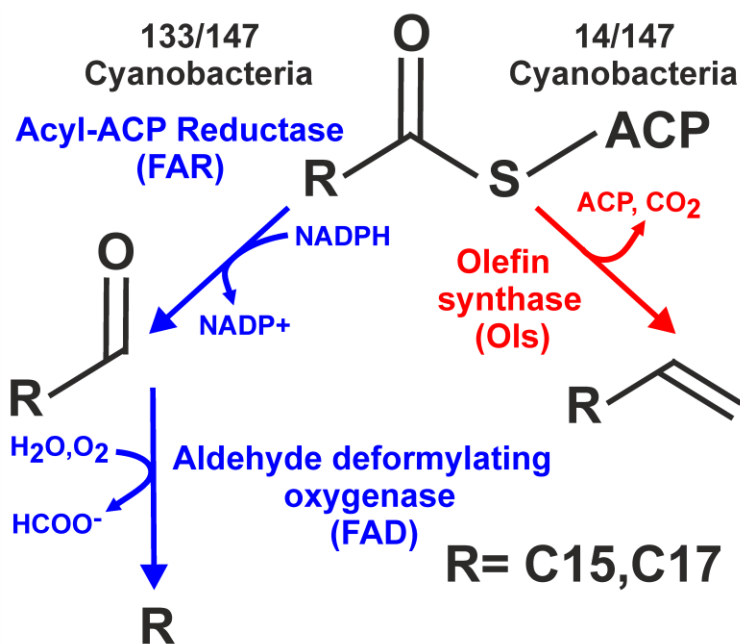
Figures

Figure 1: **Hydrocarbon biosynthesis is encoded in all sequenced cyanobacteria.** Detailed are the two hydrocarbon biosynthetic pathways, indicated in blue and red, respectively, in cyanobacteria. The number of species encoding the enzymes in each pathway is indicated.
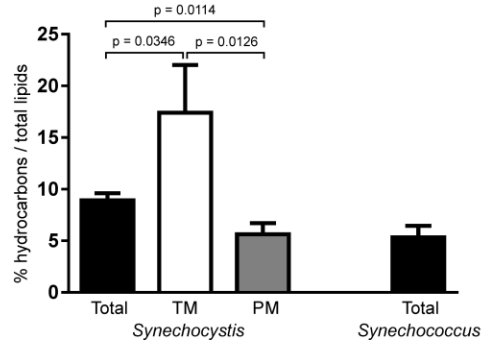
33

Figure 2: **Hydrocarbons accumulate within cyanobacterial membranes.** Detection of (A) CP47 and (B) SbtA in purified plasma and thylakoid membrane fractions (replicates 1-3). Small amounts of CP47 were consistently detected in the purified plasma membrane fractions. 5 μg protein was loaded, with antibodies diluted 1:2,000. PM: plasma membrane. TM: thylakoid membrane. (C) Percentage of hydrocarbons as total lipids in *Synechocystis* total, thylakoid and plasma membranes and *Synechocystis* total membrane samples. Results are from three biological replicates. Mean ± S.D. is indicated. Statistical significance was determined by a Student's t-test.
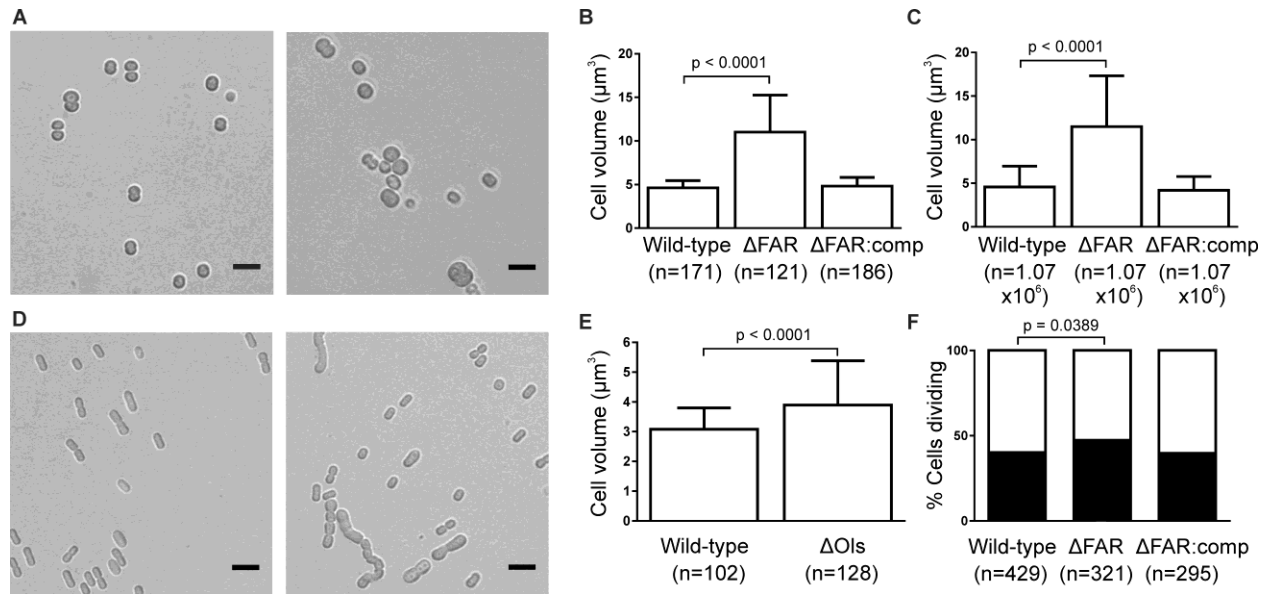
Figure 3: **Hydrocarbon deficient mutants have increased cell size and division defects.** (A) Bright-field images of wild-type *Synechocystis* (left) and ΔFAR (right) cells. Scale bars correspond to 5 µm. Cell volume of *Synechocystis* strains quantified via (B) measuring the diameter of cells from confocal microscopy images and (C) particle counting measurements. (D) Bright-field images of wild-type *Synechococcus* (left) and ΔOls (right) cells. Scale bars correspond to 5 µm. (E) Cell volume of *Synechococcus* strains quantified via measuring the width and length of cells from confocal microscopy images. (B, C, E) Mean ± S.D. is indicated. Statistical significance was determined by a Student's t-test. (F) Percentage of single versus actively dividing *Synechocystis* cells. Statistical significance was determined by a 2-way Chi-square test.
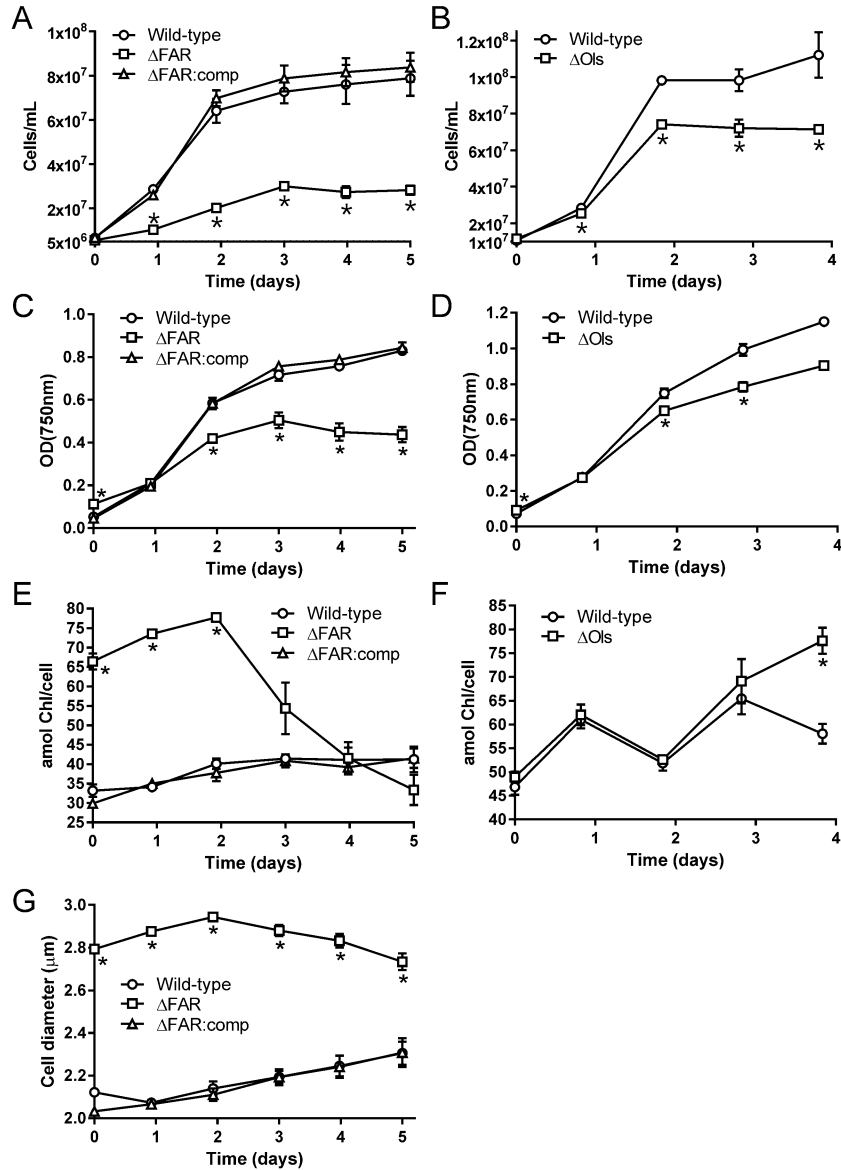
Figure 4: **Hydrocarbons are essential for optimal growth of *Synechocystis* and *Synechococcus*.** Growth of (A, C) *Synechocystis* and (B, D) *Synechococcus* under 40 μmol photons m^{-2} s^{-1} light. An equal number of cells, approximately $5x10^6$ for *Synechocystis* strains and $1x10^7$ for *Synechococcus* strains, were added to each culture. This corresponded to an OD_{750nm} equal to 0.07±0.001, 0.127±0.009 and 0.06±0.002 for wild-type *Synechocystis*, ΔFAR and ΔFAR:comp (C), respectively, and 0.076±0.003 and 0.105±0.008 for wild-type *Synechococcus* and ΔOls (D), respectively. The growth rate constants for wild-type

Synechocystis, ΔFAR and ΔFAR:comp were $1.24\pm0.20x10^6$, $3.08\pm0.13x10^5$ (p=0.0169) and $1.52\pm0.14x10^6$ cells.h^{-1}, respectively, and for wild-type *Synechococcus* and ΔOls were $1.98\pm0.02x10^6$ and $1.42\pm0.04x10^6$ cells.h^{-1} (p=0.0009), respectively. (E, F) The amount of chlorophyll per cell (in attomol) in *Synechocystis* and *Synechococcus* strains, respectively. (G) Cell diameter of *Synechocystis* strains. Results are from three biological replicates. Errors bars indicate S.D. Asterisks indicate significant differences between wild-type and hydrocarbon deficient samples (Student's paired *t* test: P < 0.05).
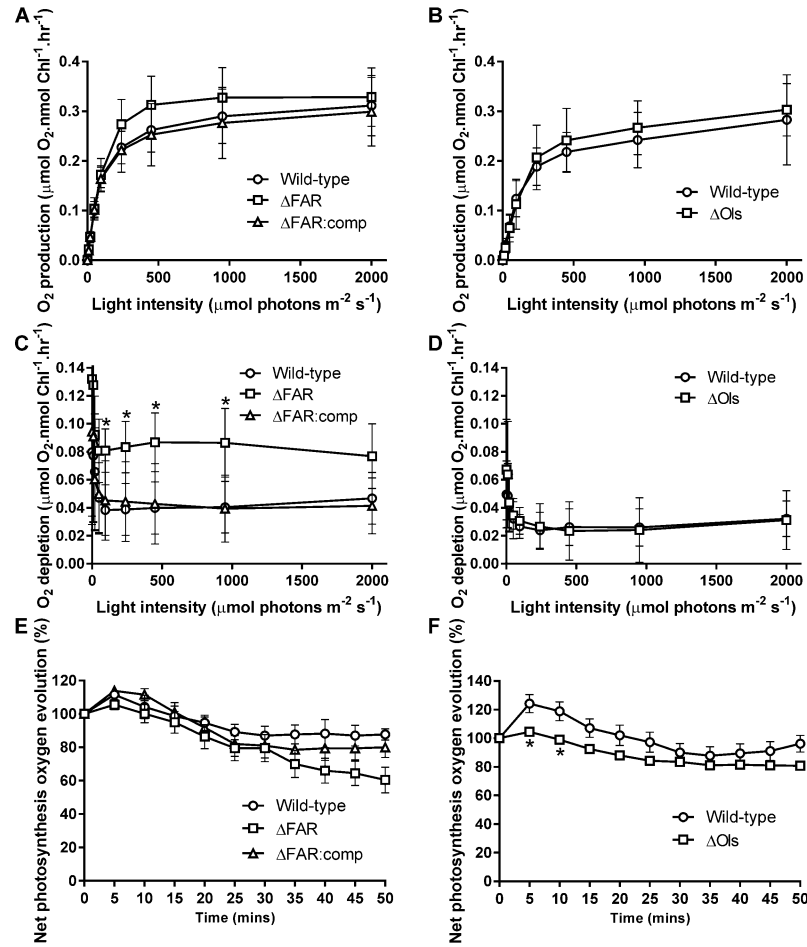
Figure 5: Photosynthetic rates and photoinhibition are similar between wild-type and hydrocarbon-deficient mutants. Oxygen evolution was measured at different light intensities in (A) *Synechocystis* and (B) *Synechococcus* to examine photosynthesis. The maximum photosynthetic rate of wild-type *Synechocystis*, ΔFAR and ΔFAR:comp was 0.311±0.025, 0.329±0.024 and 0.299±0.028 μmol O_2.nmol Chl^{-1}.hr^{-1}, respectively, and of wild-type *Synechococcus* and ΔOls was 0.283±0.03 and 0.303±0.018 μmol O_2.nmol Chl^{-1}.hr^{-1}, respectively. Respiration was determined by measuring oxygen consumption following each light period in (C) *Synechocystis* and (D) *Synechococcus*. The average oxygen consumption rate following dark periods after 95 μmol photons m^{-2} s^{-1} of wild-type *Synechocystis*, ΔFAR and

ΔFAR:comp was 0.041 ± 0.008, 0.083 ± 0.006 and 0.043 ± 0.01 μmol O_2.nmol $Chl^{-1}.hr^{-1}$, respectively, and of wild-type *Synechococcus* and ΔOls was 0.027 ± 0.005 and 0.027 ± 0.007 μmol O_2.nmol $Chl^{-1}.hr^{-1}$, respectively. Photoinhibition was determined by measuring oxygen evolution at a light intensity of (E) 2000 μmol photons $m^{-2} s^{-1}$ in *Synechocystis* and (F) 3000 μmol photons $m^{-2} s^{-1}$ in *Synechococcus*. All results are from six to nine separate biological replicates. Errors bars indicate S.D. Asterisks indicate significant differences between wild-type and hydrocarbon deficient samples (Student's paired *t* test: $P < 0.05$).
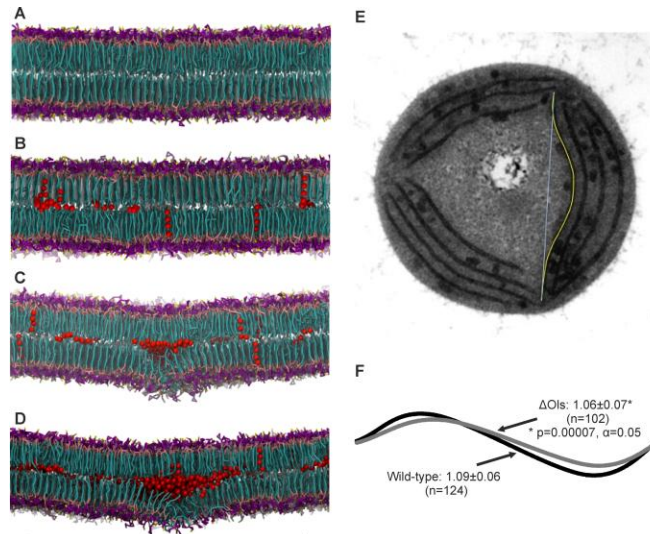
Figure 6: **Hydrocarbons disrupt membrane order by integrating into the lipid bilayer.**
Modelling of cyanobacterial membranes containing (A) 0, (B) 2.5, (C) 5 and (D) 7.5 mol heptadecane/mol total lipids in the bilayer. Hydrocarbons are shown as red van der Waals spheres. Lipids are shown in stick representation, and colored as follows: lipid head group rings are shown in magenta, phosphate beads in tan, sulfate beads in yellow, diglycerol beads in pink, and lipid tails in cyan. Snapshots show the direction of swelling associated with alkane accumulation that the membranes settled into, which was stochastic. (E) Electron micrograph of a transverse section of *Synechococcus* illustrating measurement of the curvature index, given by the ratio of the length of the membrane section (yellow line) and the shortest distance between the ends of the membrane section (cyan line) (F) Comparison of lines with curvature index derived from membrane measurements. Mean ± S.D. is indicated. Statistical significance was determined by a 2-tailed t-test. The distance of the inter-node measurements was similar between strains (Wild-type: 616±147 nm, ΔOls: 582±142 nm; 2-tailed t-test: P=0.1, α=0.05).

References

Altschul SF, Gish W, Miller W, Myers EW, Lipman DJ (1990) Basic local alignment search tool. J Mol Biol 215: 403-410

Armbruster U, Labs M, Pribil M, Viola S, Xu W, Scharfenberg M, Hertle AP, Rojahn U, Jensen PE, Rappaport F, Joliot P, Dormann P, Wanner G, Leister D (2013) *Arabidopsis* CURVATURE THYLAKOID1 proteins modify thylakoid architecture by inducing membrane curvature. Plant Cell 25: 2661-2678

Berendsen HJC, Postma JPM, Vangunsteren WF, Dinola A, Haak JR (1984) Molecular-Dynamics with Coupling to an External Bath. Journal of Chemical Physics 81: 3684-3690

Berla BM, Saha R, Maranas CD, Pakrasi HB (2015) Cyanobacterial Alkanes Modulate Photosynthetic Cyclic Electron Flow to Assist Growth under Cold Stress. Scientific Reports 5

Biller SJ, Berube PM, Berta-Thompson JW, Kelly L, Roggensack SE, Awad L, Roache-Johnson KH, Ding H, Giovannoni SJ, Rocap G, Moore LR, Chisholm SW (2014) Genomes of diverse isolates of the marine cyanobacterium *Prochlorococcus*. Scientific Data 1

Bourdenx B, Bernard A, Domergue F, Pascal S, Leger A, Roby D, Pervent M, Vile D, Haslam RP, Napier JA, Lessire R, Joubes J (2011) Overexpression of *Arabidopsis* ECERIFERUM1 promotes wax very-long-chain alkane biosynthesis and influences plant response to biotic and abiotic stresses. Plant Physiol 156: 29-45

Cabeen MT, Charbon G, Vollmer W, Born P, Ausmees N, Weibel DB, Jacobs-Wagner C (2009) Bacterial cell curvature through mechanical control of cell growth. Embo Journal 28: 1208-1219

Castenholz RW (1988) Culturing methods for Cyanobacteria. Method Enzymol 167: 68-93

Choi YJ, Lee SY (2013) Microbial production of short-chain alkanes. Nature 502: 571-+

Coates RC, Podell S, Korobeynikov A, Lapidus A, Pevzner P, Sherman DH, Allen EE, Gerwick L, Gerwick WH (2014) Characterization of cyanobacterial hydrocarbon composition and distribution of biosynthetic pathways. PLoS One 9: e85140

Davey MP, Burrell MM, Woodward FI, Quick WP (2008) Population-specific metabolic phenotypes of *Arabidopsis lyrata* ssp *petraea*. New Phytologist 177: 380-388

Davey MP, Horst I, Duong GH, Tomsett EV, Litvinenko ACP, Howe CJ, Smith AG (2014) Triacylglyceride production and autophagous responses in *Chlamydomonas reinhardtii* depend on resource allocation and carbon source. Eukaryotic Cell 13: 392-400

Dilger JP, Benz R (1985) Optical and Electrical-Properties of Thin Monoolein Lipid Bilayers. Journal of Membrane Biology 85: 181-189

Flombaum P, Gallegos JL, Gordillo RA, Rincon J, Zabala LL, Jiao N, Karl DM, Li WK, Lomas MW, Veneziano D, Vera CS, Vrugt JA, Martiny AC (2013) Present and future global distributions of the marine Cyanobacteria *Prochlorococcus* and *Synechococcus*. PNAS 110: 9824-9829

Galloway JN, Dentener FJ, Capone DG, Boyer EW, Howarth RW, Seitzinger SP, Asner GP, Cleveland CC, Green PA, Holland EA, Karl DM, Michaels AF, Porter JH, Townsend AR, Vorosmarty CJ (2004) Nitrogen cycles: past, present, and future. Biogeochemistry 70: 153-226

Graham TR, Kozlov MM (2010) Interplay of proteins and lipids in generating membrane curvature. Current Opinion in Cell Biology 22: 430-436

Heinz S, Rast A, Shao L, Gutu A, Gugel IL, Heyno E, Labs M, Rengstl B, Viola S, Nowaczyk MM, Leister D, Nickelsen J (2016) Thylakoid Membrane Architecture in *Synechocystis* Depends on CurT, a Homolog of the Granal CURVATURE THYLAKOID1 Proteins. Plant Cell

Howard RW, Blomquist GJ (2005) Ecological, behavioral, and biochemical aspects of insect hydrocarbons. Annu Rev Entomol 50: 371-393

Howard TP, Middelhaufe S, Moore K, Edner C, Kolak DM, Taylor GN, Parker DA, Lee R, Smirnoff N, Aves SJ, Love J (2013) Synthesis of customized petroleum-replica fuel molecules by targeted modification of free fatty acid pools in *Escherichia coli*. Proceedings of the National Academy of Sciences of the United States of America 110: 7636-7641

Howe CJ, Barbrook AC, Nisbet RER, Lockhart PJ, Larkum AWD (2008) The origin of plastids. Philos Trans R Soc Lond B Biol Sci 363: 2675-2685

Huang F, Parmryd I, Nilsson F, Persson AL, Pakrasi HB, Andersson B, Norling B (2002) Proteomics of *Synechocystis* sp. strain PCC 6803: identification of plasma membrane proteins. Mol Cell Proteomics 1: 956-966

Ingolfsson HI, Melo MN, van Eerden FJ, Arnarez C, Lopez CA, Wassenaar TA, Periole X, de Vries AH, Tieleman DP, Marrink SJ (2014) Lipid Organization of the Plasma Membrane. Journal of the American Chemical Society 136: 14554-14559

Kana R (2013) Mobility of photosynthetic proteins. Photosynthesis Research 116: 465-479

Kaneko T, Sato S, Kotani H, Tanaka A, Asamizu E, Nakamura Y, Miyajima N, Hirosawa M, Sugiura M, Sasamoto S, Kimura T, Hosouchi T, Matsuno A, Muraki A, Nakazaki N, Naruo K, Okumura S, Shimpo S, Takeuchi C, Wada T, Watanabe A, Yamada M, Yasuda M, Tabata S (1996) Sequence analysis of the genome of the unicellular cyanobacterium *Synechocystis* sp. strain PCC6803. II. Sequence determination of the entire genome and assignment of potential protein-coding regions (supplement). DNA Res 3: 185-209

Kosma DK, Bourdenx B, Bernard A, Parsons EP, Lu S, Joubes J, Jenks MA (2009) The impact of water deficiency on leaf cuticle lipids of *Arabidopsis*. Plant Physiol 151: 1918-1929

Kunkel DD (1982) Thylakoid Centers - Structures Associated with the Cyanobacterial Photosynthetic Membrane System. Archives of Microbiology 133: 97-99

Lea-Smith DJ, Biller SJ, Davey MP, Cotton CA, Perez Sepulveda BM, Turchyn AV, Scanlan DJ, Smith AG, Chisholm SW, Howe CJ (2015) Contribution of cyanobacterial alkane production to the ocean hydrocarbon cycle. Proc Natl Acad Sci U S A 112: 13591-13596

Lea-Smith DJ, Bombelli P, Dennis JS, Scott SA, Smith AG, Howe CJ (2014) Phycobilisome-deficient strains of *Synechocystis* sp. PCC 6803 have reduced size and require carbon-limiting conditions to exhibit enhanced productivity. Plant Physiol 165: 705-714

Lea-Smith DJ, Bombelli P, Vasudevan R, Howe CJ (2015) Photosynthetic, respiratory and extracellular electron transport pathways in cyanobacteria. Biochim Biophys Acta

Lea-Smith DJ, Ross N, Zori M, Bendall DS, Dennis JS, Scott SA, Smith AG, Howe CJ (2013) Thylakoid terminal oxidases are essential for the cyanobacterium *Synechocystis* sp. PCC 6803 to survive rapidly changing light intensities. Plant Physiol 162: 484-495

Lea-Smith DJ, Vasudevan R, Howe CJ (2016) Generation of Marked and Markerless Mutants in Model Cyanobacterial Species. J Vis Exp

Li N, Chang WC, Warui DM, Booker SJ, Krebs C, Bollinger JM, Jr. (2012) Evidence for only oxygenative cleavage of aldehydes to alk(a/e)nes and formate by cyanobacterial aldehyde decarbonylases. Biochemistry 51: 7908-7916

Lopez CA, Sovova Z, van Eerden FJ, de Vries AH, Marrink SJ (2013) Martini Force Field Parameters for Glycolipids. Journal of Chemical Theory and Computation 9: 1694-1708

Manna M, Rog T, Vattulainen I (2014) The challenges of understanding glycolipid functions: An open outlook based on molecular simulations. Biochimica Et Biophysica Acta-Molecular and Cell Biology of Lipids 1841: 1130-1145

Marrink SJ, de Vries AH, Tieleman DP (2009) Lipids on the move: Simulations of membrane pores, domains, stalks and curves. Biochimica Et Biophysica Acta-Biomembranes 1788: 149-168

Marrink SJ, Risselada HJ, Yefimov S, Tieleman DP, de Vries AH (2007) The MARTINI force field: Coarse grained model for biomolecular simulations. Journal of Physical Chemistry B 111: 7812-7824

McMahon HT, Gallop JL (2005) Membrane curvature and mechanisms of dynamic cell membrane remodelling. Nature 438: 590-596

Mendez-Perez D, Begemann MB, Pfleger BF (2011) Modular synthase-encoding gene involved in alpha-olefin biosynthesis in *Synechococcus* sp. strain PCC 7002. Appl Environ Microbiol 77: 4264-4267

Merzlyak MN, Naqvi KR (2000) On recording the true absorption spectrum and the scattering spectrum of a turbid sample: application to cell suspensions of the cyanobacterium *Anabaena variabilis*. J Photochem Photobiol B 58: 123-129

Mohamed HE, Vermaas W (2004) Slr1293 in *Synechocystis* sp. strain PCC 6803 Is the C-3',4' desaturase (CrtD) involved in myxoxanthophyll biosynthesis. J Bacteriol 186: 5621-5628

Murata N, Wada H, Gombos Z (1992) Modes of Fatty-Acid Desaturation in Cyanobacteria. Plant and Cell Physiology 33: 933-941

Murphy DJ (1982) The Importance of Non-Planar Bilayer Regions in Photosynthetic Membranes and Their Stabilization by Galactolipids. Febs Letters 150: 19-26

Norling B, Zak E, Andersson B, Pakrasi H (1998) 2D-isolation of pure plasma and thylakoid membranes from the cyanobacterium *Synechocystis* sp. PCC 6803. FEBS Lett 436: 189-192

Nurnberg DJ, Mariscal V, Parker J, Mastroianni G, Flores E, Mullineaux CW (2014) Branching and intercellular communication in the Section V cyanobacterium *Mastigocladus laminosus*, a complex multicellular prokaryote. Molecular Microbiology 91: 935-949

Porra RJ, Thompson WA, Kriedemann PE (1989) Determination of Accurate Extinction Coefficients and Simultaneous-Equations for Assaying Chlorophyll-a and Chlorophyll-B Extracted with 4 Different Solvents - Verification of the Concentration of Chlorophyll Standards by Atomic-Absorption Spectroscopy. Biochimica Et Biophysica Acta 975: 384-394

Raven JA (1998) The twelfth Tansley Lecture. Small is beautiful: the picophytoplankton. Functional Ecology 12: 503-513

Rexroth S, Mullineaux CW, Ellinger D, Sendtko E, Rögner M, Koenig F (2011) The plasma membrane of the Cyanobacterium *Gloeobacter violaceus* contains segregated bioenergetic domains. Plant Cell 23: 2379-2390

Reynolds ES (1963) Use of Lead Citrate at High Ph as an Electron-Opaque Stain in Electron Microscopy. Journal of Cell Biology 17: 208-&

Ried JL, Collmer A (1987) An nptI-sacB-sacR cartridge for constructing directed, unmarked mutations in gram-negative bacteria by marker exchange-eviction mutagenesis. Gene 57: 239-246

Rippka R, Waterbury J, Cohenbazire G (1974) Cyanobacterium Which Lacks Thylakoids. Archives of Microbiology 100: 419-436

Saw JHW, Schatz M, Brown MV, Kunkel DD, Foster JS, Shick H, Christensen S, Hou SB, Wan XH, Donachie SP (2013) Cultivation and Complete Genome Sequencing of *Gloeobacter kilaueensis* sp nov., from a Lava Cave in Kilauea Caldera, Hawai'i. PLoS One 8

Schirmer A, Rude MA, Li X, Popova E, del Cardayre SB (2010) Microbial biosynthesis of alkanes. Science 329: 559-562

Sheng J, Vannela R, Rittrnann BE (2011) Evaluation of methods to extract and quantify lipids from *Synechocystis* PCC 6803. Bioresource Technology 102: 1697-1703

Shipley GG, Green JP, Nichols BW (1973) The phase behavior of monogalactosyl, digalactosyl, and sulphoquinovosyl diglycerides. Biochim Biophys Acta 311: 531-544

Sorigue D, Legeret B, Cuine S, Morales P, Mirabella B, Guedeney G, Li-Beisson Y, Jetter R, Peltier G, Beisson F (2016) Microalgae synthesize hydrocarbons from long-chain fatty acids via a light-dependent pathway. Plant Physiol

Stengel A, Gugel IL, Hilger D, Rengstl B, Jung H, Nickelsen J (2012) Initial steps of photosystem II de novo assembly and preloading with manganese take place in biogenesis centers in *Synechocystis*. Plant Cell 24: 660-675

Stingaciu LR, O'Neill H, Liberton M, Urban VS, Pakrasi HB, Ohl M (2016) Revealing the Dynamics of Thylakoid Membranes in Living Cyanobacterial Cells. Scientific Reports 6

Tan X, Yao L, Gao Q, Wang W, Qi F, Lu X (2011) Photosynthesis driven conversion of carbon dioxide to fatty alcohols and hydrocarbons in cyanobacteria. Metab Eng 13: 169-176

Tang EPY, Peters RH (1995) The Allometry of Algal Respiration. Journal of Plankton Research 17: 303-315

Tilcock CP (1986) Lipid polymorphism. Chem Phys Lipids 40: 109-125

Valentine DL, Reddy CM (2015) Latent hydrocarbons from cyanobacteria. Proceedings of the National Academy of Sciences of the United States of America 112: 13434-13435

van Eerden FJ, de Jong DH, de Vries AH, Wassenaar TA, Marrink SJ (2015) Characterization of thylakoid lipid membranes from cyanobacteria and higher plants by molecular dynamics simulations. Biochim Biophys Acta 1848: 1319-1330

Vattulainen I, Rog T (2011) Lipid Simulations: A Perspective on Lipids in Action. Cold Spring Harb Perspect Biol 3

Vieira J, Messing J (1982) The pUC plasmids, an M13mp7-derived system for insertion mutagenesis and sequencing with synthetic universal primers. Gene 19: 259-268

White SH, King GI, Cain JE (1981) Location of Hexane in Lipid Bilayers Determined by Neutron-Diffraction. Nature 290: 161-163

Wu LJ, Errington J (2012) Nucleoid occlusion and bacterial cell division. Nature Reviews Microbiology 10: 8-12

Xu H, Vavilin D, Funk C, Vermaas W (2004) Multiple deletions of small Cab-like proteins in the cyanobacterium *Synechocystis* sp. PCC 6803: consequences for pigment biosynthesis and accumulation. J Biol Chem 279: 27971-27979

Zhou XX, Halladin DK, Rojas ER, Koslover EF, Lee TK, Huang KC, Theriot JA (2015) Mechanical crack propagation drives millisecond daughter cell separation in *Staphylococcus aureus*. Science 348: 574-578

Zwirglmaier K, Jardillier L, Ostrowski M, Mazard S, Garczarek L, Vaulot D, Not F, Massana R, Ulloa O, Scanlan DJ (2008) Global phylogeography of marine *Synechococcus* and *Prochlorococcus* reveals a distinct partitioning of lineages among oceanic biomes. Environ Microbiol 10: 147-161
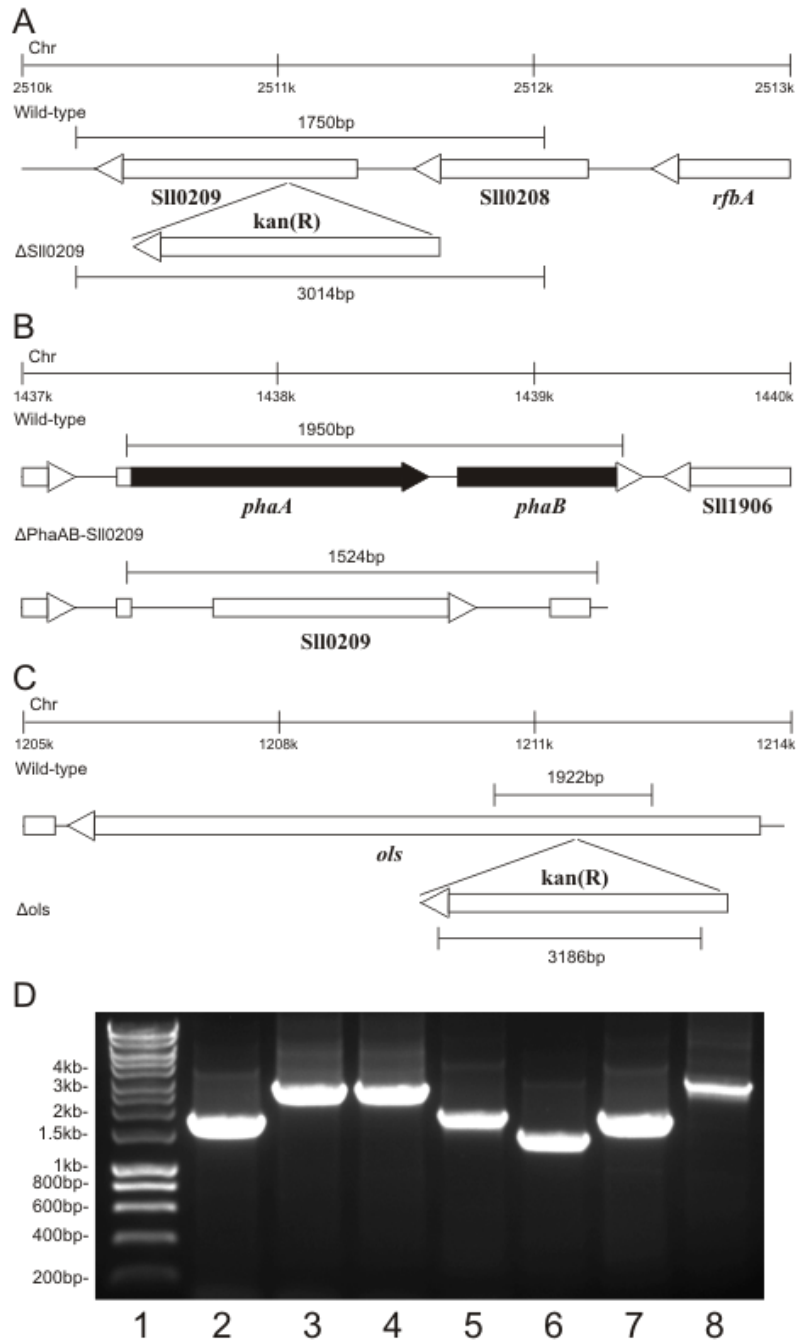
Figure S1: Generation of mutant strains in *Synechocystis* and *Synechococcus*. Schematic representations of locus location in the genome (top), and the wild-type and mutant strain (bottom) profiles expected in (A) ΔFAR (ΔSll0209), (B) Complemented (ΔFAR:comp) and (C)

ΔOls strains following amplification with primers flanking the deleted/inserted sequence. Regions deleted in ΔFAR:comp are shaded in black. (D) Amplification of genomic DNA in wild-type *Synechocystis* (Lane 2) and ΔFAR (Lane 3) and ΔFAR:comp (Lane 4) using Sll0209for/Sll0209rev primers; in wild-type *Synechocystis* (Lane 5) and ΔFAR:comp (Lane 6) using Phafor/Pharev primers; in wild-type *Synechococcus* (Lane 7) and ΔOls (Lane 8) using Olsfor/Olsrev primers. Markers are in lane 1.
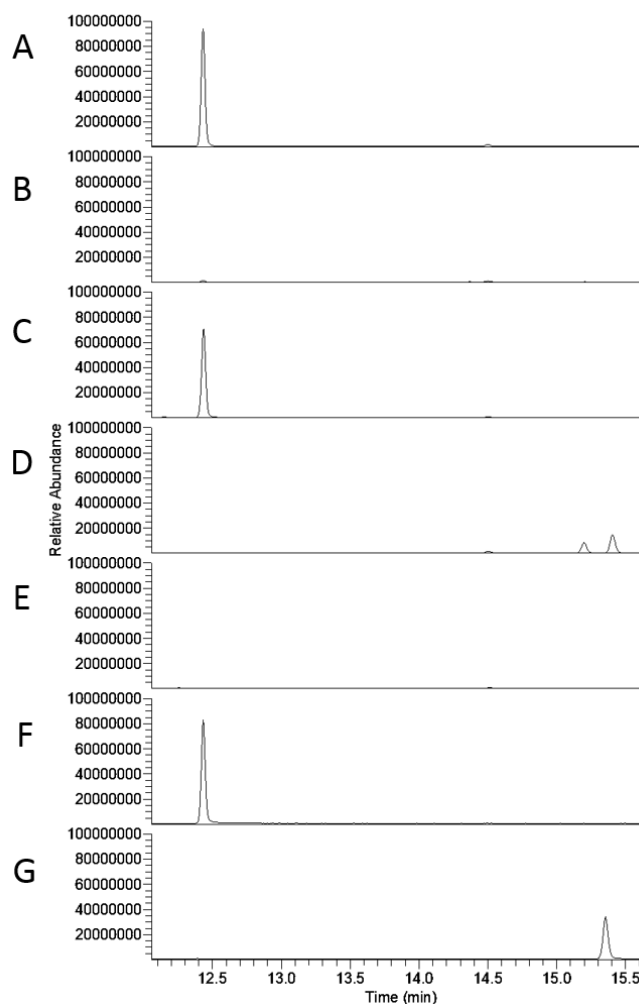
Figure S2: Chromatograms showing separation of hydrocarbons from whole cells. Hydrocarbons were extracted from (A) *Synechocystis* wild-type; (B) ΔFAR; (C) ΔFAR:comp; (D) *Synechococcus* wild-type; (E) ΔOls; (F) heptadecane standard 0.0039 mg/mL; (G) nonadecene standard 0.0038 mg/mL by GC-MS (Thermo Scientific Trace GC 1310 – ISQ LT Single Quadruple EI MS, A1-1310 Autosampler) using a Thermo TG-SQC GC column (15 m × 0.25 mm, 0.25-µm film thickness). Peaks were identified as (12.43 min) heptadecane and 15.41 min) nonadecene. 8-heptadecene was detected at 12.15 min but is not visible due to scaling. The peak at 15.2 minutes in (D) *Synechococcus* wild-type was identified (by nist library) as a hexadecan-1-ol.
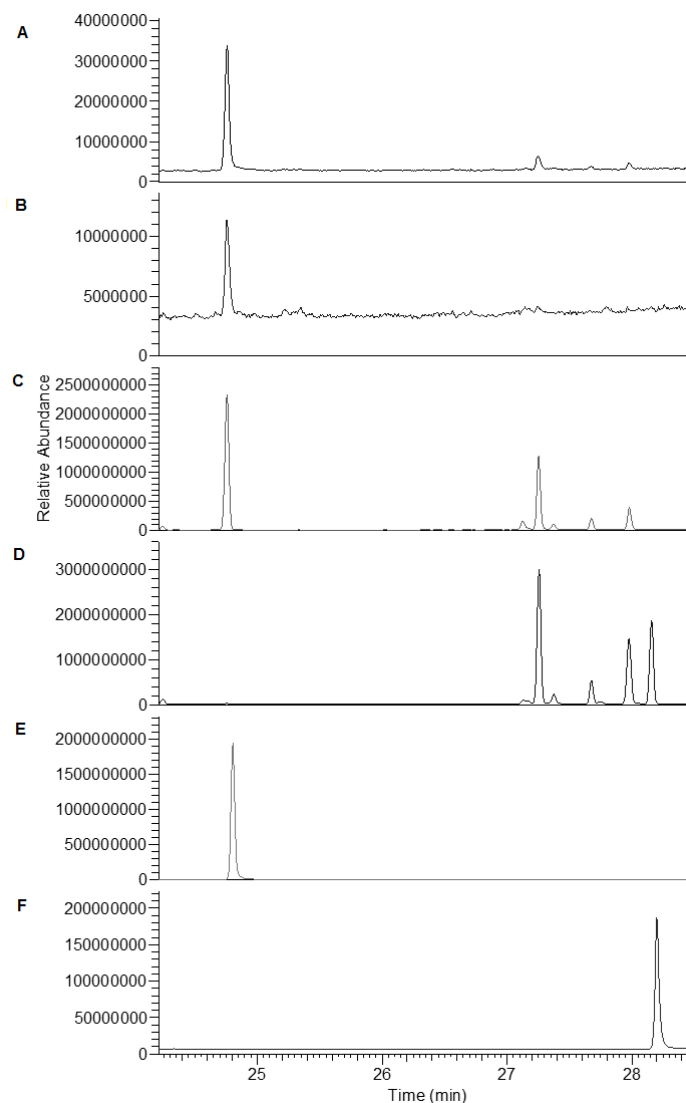
Figure S3: Chromatograms showing separation of hydrocarbons from membrane fractions. Hydrocarbons were extracted from *Synechocystis* wild-type (A) thylakoid membrane; (B) cytoplasmic membrane; (C) total membrane and (D) *Synechococcus* wild-type total membrane fractions; (E) heptadecane standard; (F) nonadecene standard GC-MS (Thermo Scientific Trace GC 1310 – ISQ LT Single Quadruple EI MS, A1-1310 Autosampler) using a Phenomenex Zebron ZB-5MSi Capillary GC Column (30m x 0.25mm x 0.25 µm). Peaks were identified as (24.76 min) heptadecane and 28.27 min) nonadecene. 8-heptadecene was detected at 24.34 min but is not visible due to scaling.
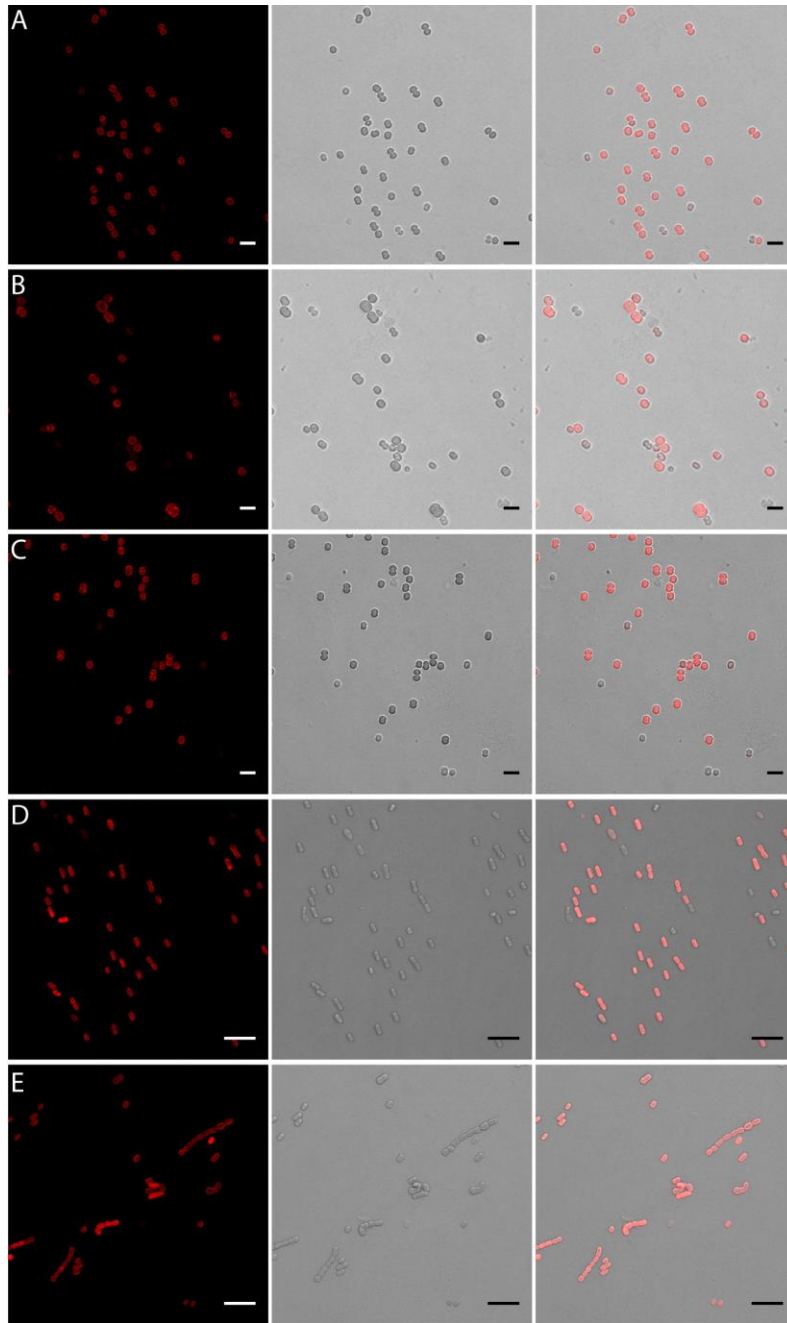
Figure S4: Brightfield confocal images of *Synechocystis* and *Synechococcus* strains. Cell morphology of strains used in this study. (A) wild-type *Synechocystis*, (B) ΔFAR and (C) ΔFAR:comp. Scale bars, 5 μm. (D) wild-type *Synechococcus* and (E) ΔOls. Scale bars, 10 μm. Images show autofluorescence (red, left), bright-field (grey, middle) and an overlay of both (right).
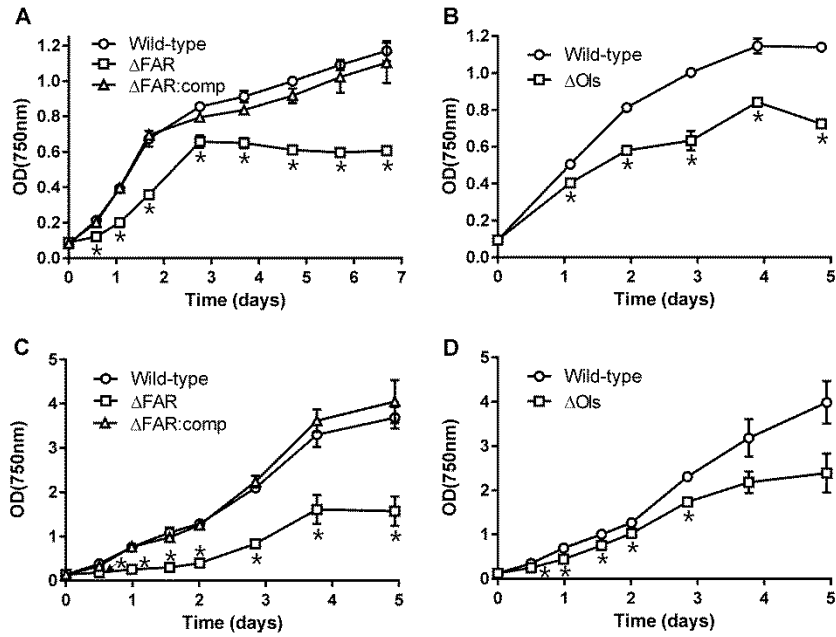
Figure S5: **Growth of *Synechocystis* and *Synechococcus* under moderate and high light.** Growth of (A, C) *Synechocystis* and (B, D) *Synechococcus* strains was measured at an OD_{750nm} under (A, B) moderate (40 µmol photons m^{-2} s^{-1}) and (C, D) high (120 µmol photons m^{-2} s^{-1}) light. Cultures were inoculated with a similar amount of cyanobacteria as measured by optical density. Samples grown under high light were bubbled with air. From strains cultured under moderate light the growth rate constants (µ) of wild-type *Synechocystis,* ΔFAR and ΔFAR:comp were 0.015 ± 0.002, 0.007 ± 0.0003 and 0.015 ± 0.001 hr^{-1}, respectively, and in wild-type *Synechococcus* and ΔOls were 0.027 ± 0.001 and 0.019 ± 0.001 hr^{-1}, respectively. From strains cultured under high light the growth rate constants (µ) of wild-type *Synechocystis,* ΔFAR and ΔFAR:comp were 0.035 ± 0.005, 0.016 ± 0.005 and 0.038 ± 0.005 hr^{-1}, respectively, and in wild-type *Synechococcus* and ΔOls were 0.034 ± 0.008 and 0.023 ± 0.005 hr^{-1}, respectively. Results are from three biological replicates. Errors bars indicate S.D. Asterisks indicate significant differences between wild-type and hydrocarbon deficient samples (Student's paired *t* test: P < 0.05).
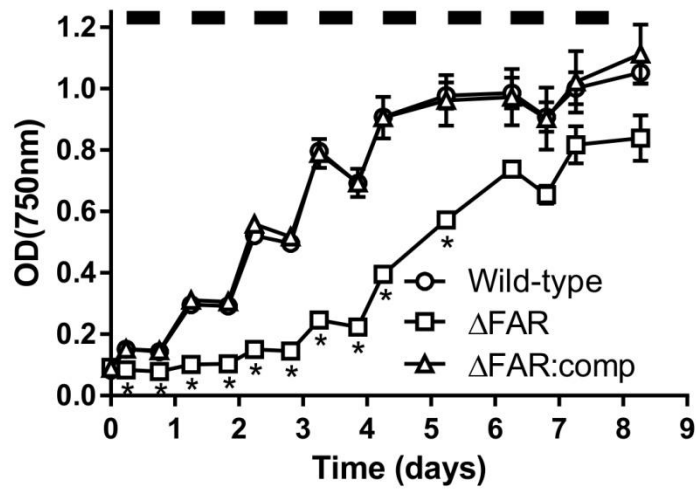
Figure S6: **Growth of *Synechocystis* under moderate light/dark cycles.** Growth of *Synechocystis* was measured at an OD of 750 nm under 12 hour light (40 μmol photons m^{-2} s^{-1})/12 hour dark cycles. The growth rate constants (μ) of wild-type *Synechocystis*, ΔFAR and ΔFAR:comp were 0.011±0.0003, 0.003±0.0001 and 0.011±0.0001 hr^{-1}. Dark periods are indicated by black bars. Results are from three biological replicates. Errors bars indicate S.D. Asterisks indicate significant differences between wild-type and hydrocarbon deficient samples (Student's paired *t* test: P < 0.05).
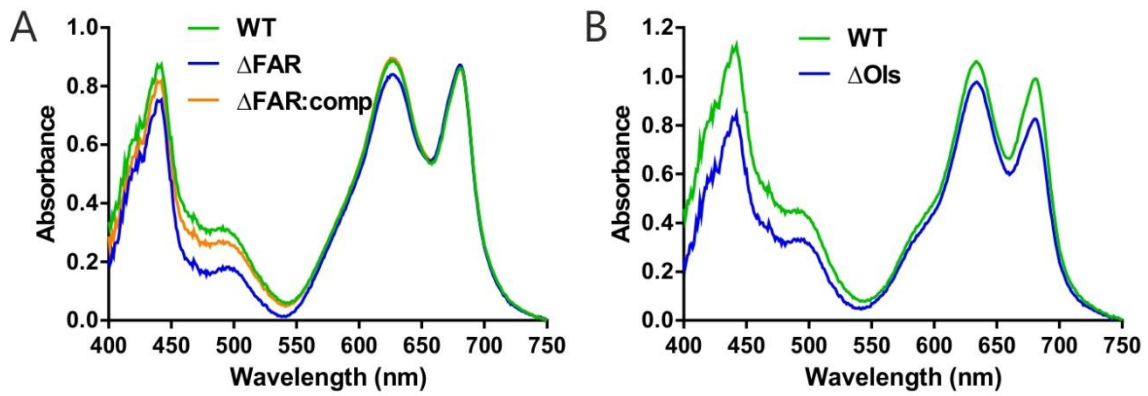
Figure S7: **Absorbance profiles of *Synechocystis* and *Synechococcus* strains.** Spectrum showing the absorbance profile of (A) *Synechocystis* and (B) *Synechococcus* cells. Values are averages from four biological replicates and are standardized to 750 nm.
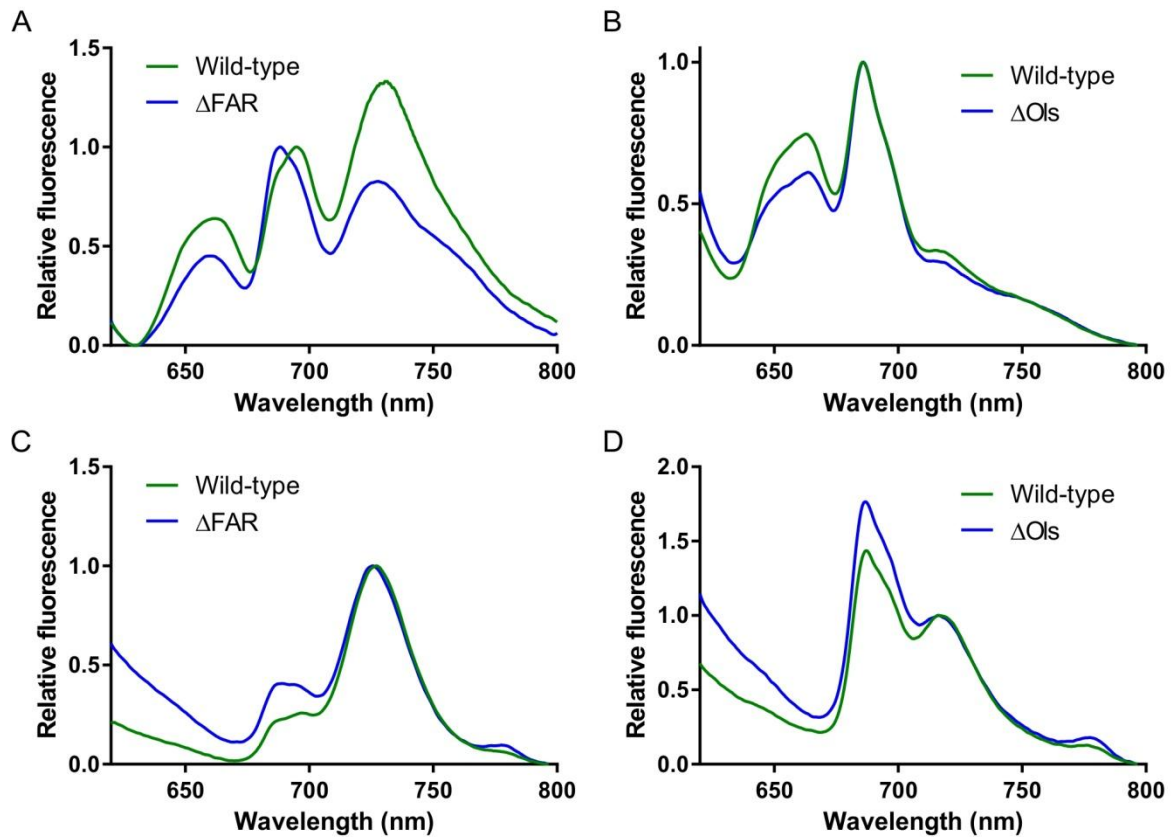
Figure S8: **77K fluorescence of *Synechocystis* and *Synechococcus* strains.** The fluorescence emission spectra of (A) *Synechocystis* and (B) *Synechococcus* cells were recorded with an excitation wavelength at 600 nm at 77K. The spectra were normalized to the highest peak between 625 and 710 nm. The fluorescence emission spectra of (C) *Synechocystis* and (D) *Synechococcus* cells were recorded with an excitation wavelength at 435 nm at 77K. The spectra were normalized to the highest peak between 710 and 750 nm. Results are representative of 3 biological replicates.

Figure S9: CG topologies of representative lipids of the membrane. These are overlaid on atomistic topologies of the same lipids. Labels refer to Martini bead type used to describe relevant interactions.

Partial density   Order parameters   Memb. organisation

no alkane

1.5 mol %

2.5 mol %

5.0 mol %

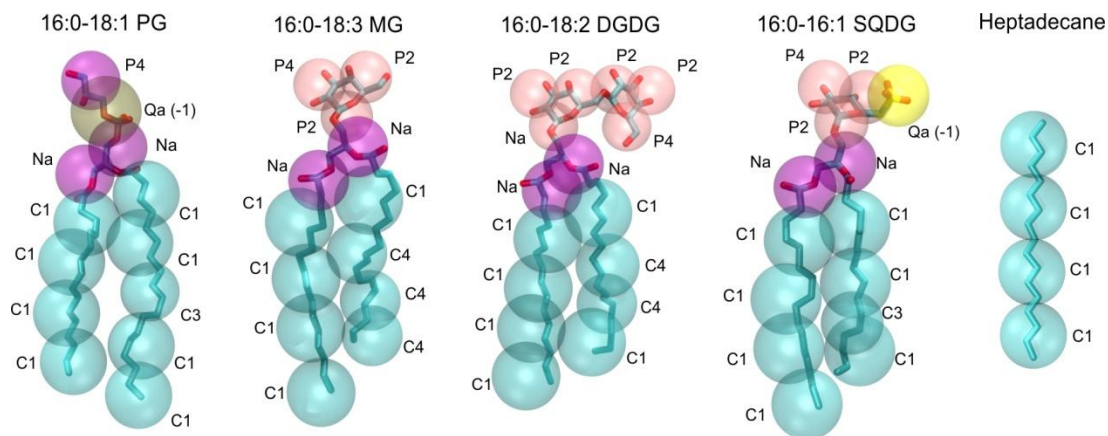7.5 mol %

7.5 mol %
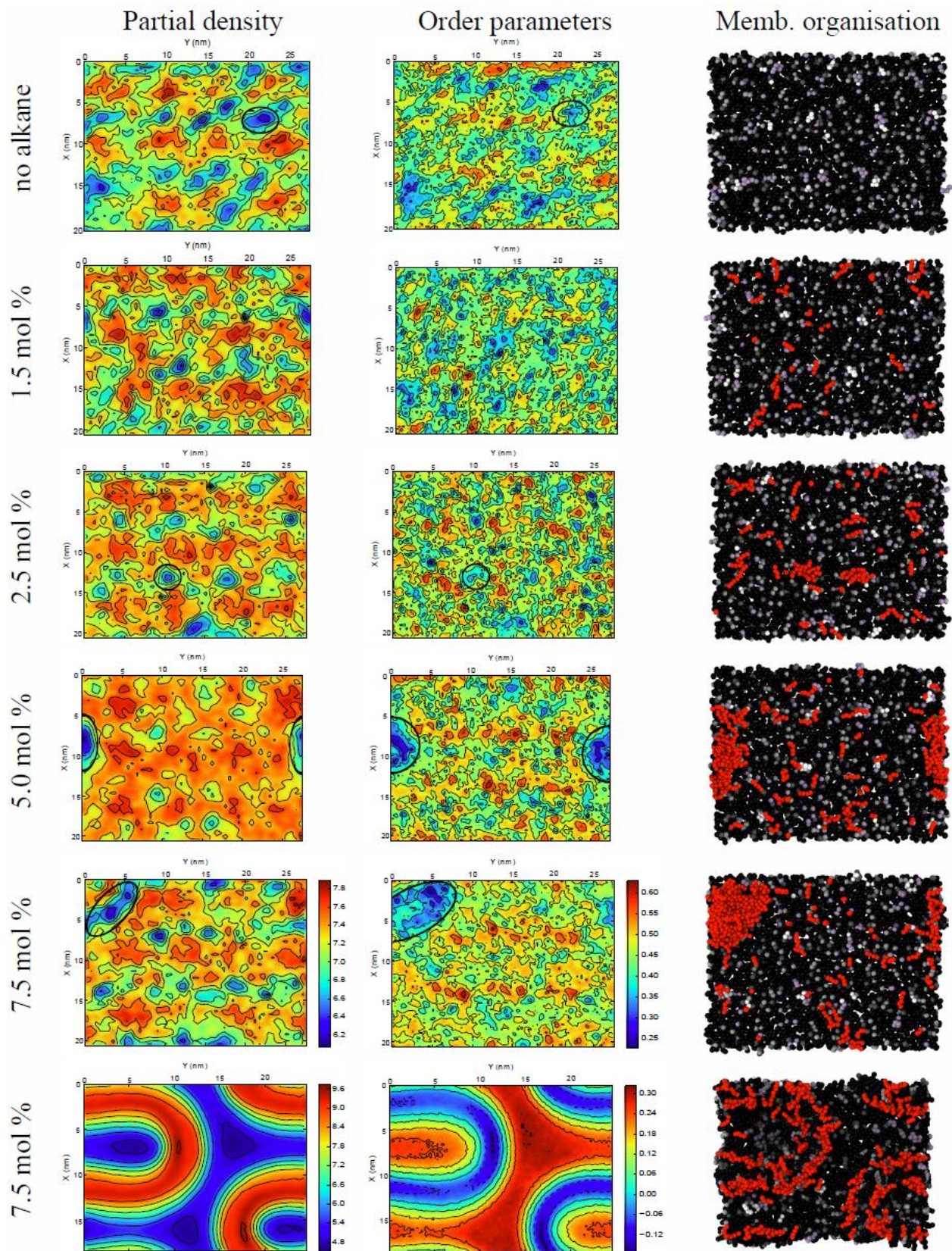
Figure S10: Membrane partial density (left panels), lipid acyl chain order parameter (central panel), and organization (right panel) in differing hydrocarbon contents averaged over the last 2 μs of simulation, seen as a bilayer landscape. In the 7.5 mol % lamellar system, these properties are shown for the first 1.2 μs of simulation, before phase transition. Regions of accumulated alkane molecules are highlighted as circles. In membrane snapshots only the tail beads are visualized, and colored according to degree of saturation. 16:0 tails are black, 16:1 grey, 18:1 white, 18:2 ice blue and 18:3 pale blue. Hydrocarbon is shown in red van der Waals representation and overlaid on the membranes for clarity.
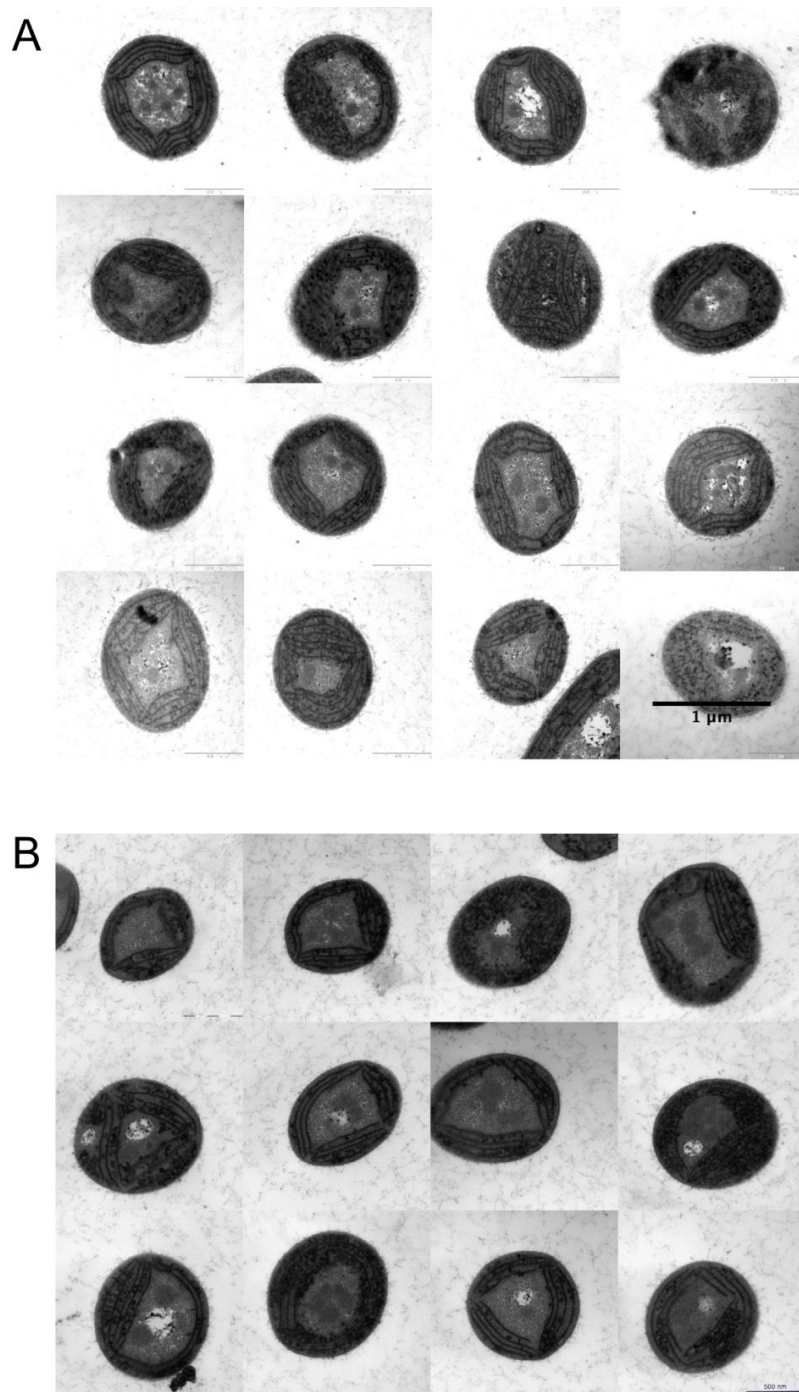
Figure S11: Electron microscopy images of *Synechococcus* cells. Transverse sections of (A) wild-type *Synechococcus* and (B) ΔOls cells used for measuring curvature.
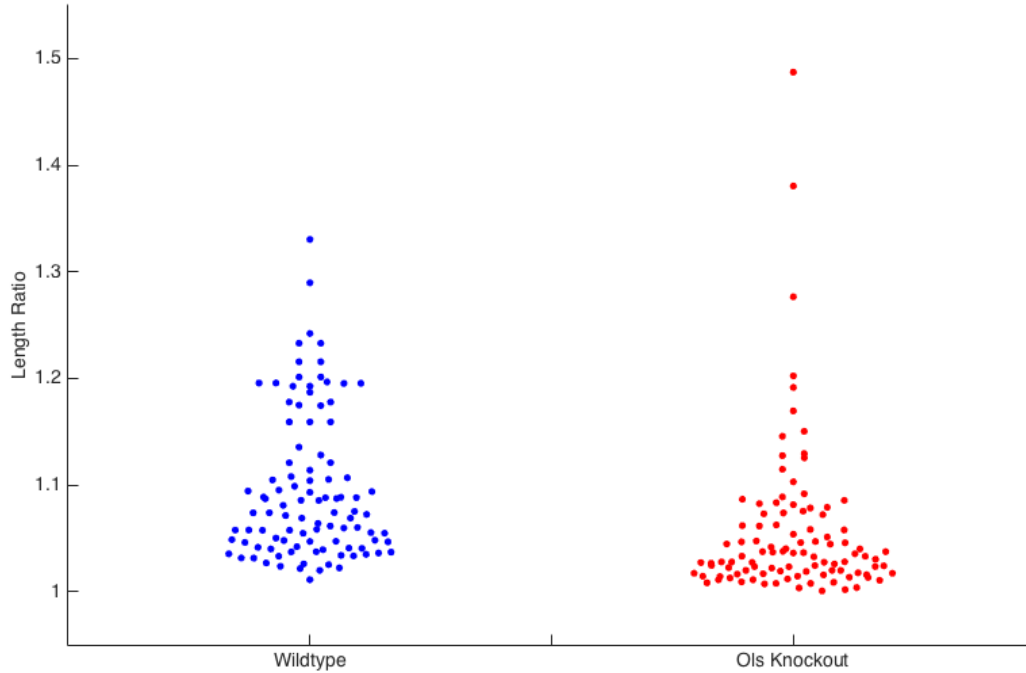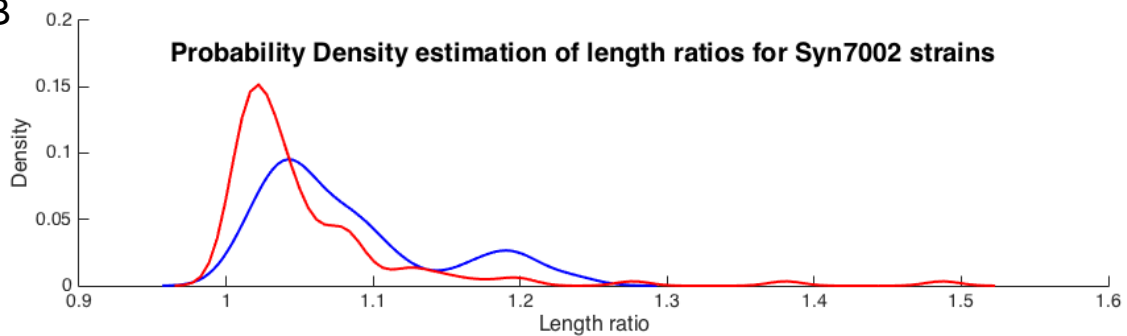
Figure S12: Length ratios (curvatures) of membranes from Synechococcus 7002 strains – Wild-type (blue) and ΔOls (red). A) Categorical scatter plot of length ratios of all membranes sampled. B) Kernel Density Plots of Length ratios from wild-type (blue) and ΔOls (red) membranes.
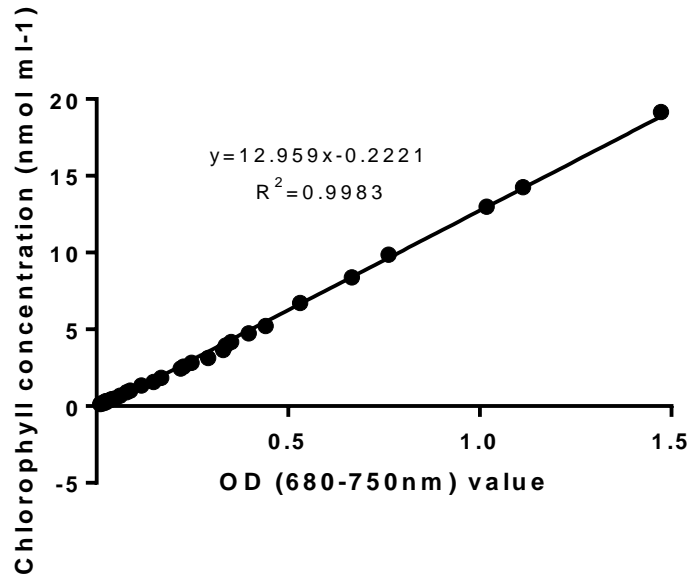
Figure S13: **Correlation between the absorbance at 680nm and 750nm, and amounts of chlorophyll measured following methanol extraction.** Twenty-nine samples were measured at an absorbance of 750nm and 680nm, followed by extraction with methanol to measure chlorophyll concentration. The amount of chlorophyll was correlated with absorbance (A_{680nm}-A_{750nm}). The regression line is shown. The slope of the regression line (R^2=0.9983), equivalent to 12.959, was calculated.

Table S1. Conservation of hydrocarbon biosynthetic pathway proteins and Curt in sequenced cyanobacteria strains. The *Synechocystis* FAD/FAR/Curt and *Synechococcus* Ols amino acid sequences were subjected to BLAST analysis against sequenced cyanobacterial genomes in the NCBI database. The positive values of these BLAST results are listed. Due to similarities between Ols and other polyketide synthase proteins only matches greater than 50% identity over the length of the query sequence are shown.

Strain	*fad*	*far*	*ols*	*curt*
Acaryochloris marina MBIC11017	292/337(86%)	191/230(83%)		55/92(60%)
Anabaena cylindrica PCC7122	301/338(89%)	197/223(88%)		82/124(66%)
Anabaena sp. 90	297/338(87%)	196/223(87%)		90/137(66%)
Anabaena sp. PCC7108	302/338(89%)	197/223(88%)		91/138(66%)
Anabaena variabilis ATCC29413	305/338(90%)	204/230(88%)		90/138(65%)
Arthrospira maxima CS-328	295/338(87%)	206/231(89%)		90/134(67%)
Arthrospira platensis NIES-39	295/338(87%)	206/231(89%)		87/134(65%)
Calothrix sp. PCC6303	298/338(88%)	202/228(88%)		81/123(66%)
Calothrix sp. PCC7103	295/338(87%)	198/219(90%)		87/135(64%)
Calothrix sp. PCC7507	299/338(88%)	202/228(88%)		82/123(67%)
Candidatus atelocyanobacterium thalassa	296/338(87%)	198/228(86%)		81/105(77%)
Chamaesiphon minutus PCC6605	299/340(87%)	193/230(83%)		69/100(69%)
Chlorogloeopsis fritschii	297/338(87%)	202/231(87%)		79/123(64%)
Chroococcales CENA595	300/338(88%)	199/230(86%)		81/119(68%)
Chroococcidiopsis thermalis PCC7203	301/339(88%)	200/228(87%)		69/95(73%)
Coleofasciculus chthonoplastes PCC7420	298/338(88%)	199/230(86%)		83/111(75%)
Crinalium epipsammum PCC9333	299/339(88%)	190/225(84%)		89/126(71%)
Crocosphaera watsonii WH8501	291/339(85%)	206/231(89%)		98/134(73%)
Cyanobacterium aponinum PCC10605	290/340(85%)	193/225(85%)		88/133(66%)
Cyanobium gracile PCC6307	256/337(75%)	181/220(82%)		36/65(55%)
Cyanobium sp. PCC7001	261/334(78%)	182/220(82%)		
Cyanothece sp. ATCC51142	294/339(86%)	206/228(90%)		99/134(74%)
Cyanothece sp. CCY0110	301/338(89%)	207/230(90%)		94/134(70%)
Cyanothece sp. PCC7424			1871/2798(66%)	98/136(72%)
Cyanothece sp. PCC7425	290/338(85%)	196/230(85%)		74/121(61%)
Cyanothece sp. PCC7822			1873/2800(66%)	88/113(78%)
Cyanothece sp. PCC8801	306/339(90%)	205/230(89%)		95/131(73%)
Cylindrospermopsis raciborskii CS-505	301/338(89%)	191/222(86%)		88/136(65%)
Cylindrospermum stagnale PCC7417	299/338(88%)	199/231(86%)		92/137(67%)

Dactylococcopsis salina PCC8305	282/338(83%)	199/231(86%)		77/105(73%)
Dolichospermum circinale	298/338(88%)	197/221(89%)		78/115(68%)
Fischerella sp. PCC9339	296/338(87%)	200/228(87%)		68/117(58%)
Fischerella sp. PCC9431	296/338(87%)	200/228(87%)		69/117(59%)
Fischerella sp. PCC9605	299/338(88%)	203/228(89%)		81/123(66%)
Geitlerinema sp. PCC7407	292/339(86%)	204/231(88%)		75/104(72%)
Geminocystis herdmanii			1791/2846(62%)	76/105(72%)
Geminocystis sp. NIES-3708	292/340(85%)	199/230(86%)		92/137(67%)
Geminocystis sp. NIES-3709			1785/2865(62%)	87/136(64%)
Gloeobacter kilaueensis JS1	264/340(78%)	179/221(81%)		
Gloeobacter violaceus PCC7421	266/338(79%)	183/221(82%)		
Gloeocapsa sp. PCC7428	299/338(88%)	193/226(85%)		88/130(68%)
Halothece sp. PCC7418	287/338(84%)	202/228(88%)		66/95(69%)
Hassallia byssoidea VB512170	297/338(87%)	200/228(87%)		84/124(68%)
Leptolyngbya boryana	295/338(87%)	200/230(86%)		76/111(68%)
Leptolyngbya sp. JSC-1	294/338(86%)	201/230(87%)		89/136(65%)
Leptolyngbya sp. PCC7376			2161/2726(79%)	87/134(65%)
Limnorpahis robusta	297/338(87%)	204/231(88%)		71/94(76%)
Lyngbya aestuarii	298/338(88%)	201/230(87%)		91/153(59%)
Lyngbya sp. PCC8106	296/338(87%)	196/229(85%)		88/143(62%)
Mastigocoleus repens	294/338(86%)	201/230(87%)		82/123(67%)
Mastigocoleus testarum	296/338(87%)	202/228(88%)		
Microchaete sp. PCC7126	298/338(88%)	206/230(89%)		86/138(62%)
Microcoleus sp. PCC7113	301/340(88%)	201/230(87%)		95/142(67%)
Microcoleus vaginatus FGP-2	297/338(87%)	194/230(84%)		73/101(72%)
Microcystis aeruginosa NIES-843	299/338(88%)	207/231(89%)		77/110(70%)
Moorea producens 3L			1558/2851(55%)	91/137(66%)
Myxosarcina sp. Gl1			1820/2823(64%)	73/111(66%)
Nodularia spumigena CCY9414	302/338(89%)	199/230(86%)		91/137(66%)
Nostoc azollae' 0708	299/338(88%)	197/223(88%)		91/140(65%)
Nostoc punctiforme PCC73102	298/338(88%)	196/222(88%)		91/141(65%)
Nostoc sp. KNUA003	307/338(90%)	197/230(85%)		
Nostoc sp. PCC6720	307/338(90%)	197/230(85%)		
Nostoc sp. PCC7107	305/338(90%)	195/230(84%)		91/137(66%)
Nostoc sp. PCC7120	305/338(90%)	204/230(88%)		90/138(65%)
Nostoc sp. PCC7524	303/338(89%)	202/230(87%)		88/137(64%)
Oscillatoria acuminata PCC6304	294/338(86%)	202/231(87%)		77/110(70%)
Oscillatoria cyanobacterium JSC-12	297/339(87%)	201/230(87%)		85/123(69%)
Oscillatoria nigro-viridis PCC7112	297/338(87%)	194/230(84%)		73/101(72%)
Oscillatoria sp. PCC6506	301/338(89%)	196/230(85%)		87/134(65%)
Oscillatoria sp. PCC10802	295/341(86%)	202/231(87%)		89/134(66%)
Pleurocapsa sp. PCC7319			1862/2843(65%)	83/135(61%)

Pleurocapsa sp. PCC7327			1890/2861(66%)	91/110(83%)
Prochlorococcus marinus str. AS9601	262/337(77%)	173/214(80%)		37/68(54%)
Prochlorococcus marinus str. CCMP1375	263/337(78%)	169/218(77%)		60/114(53%)
Prochlorococcus marinus str. CCMP1986	261/337(77%)	173/214(80%)		32/63(51%)
Prochlorococcus EQPAC1	261/337(77%)	173/214(81%)		32/63(51%)
Prochlorococcus GP2	262/337(78%)	173/214(81%)		53/114(46%)
Prochlorococcus LG	263/337(78%)	169/218(78%)		60/114(53%)
Prochlorococcus marinus str. MIT9107	258/337(77%)	171/214(80%)		53/114(46%)
Prochlorococcus marinus str. MIT9116	258/337(77%)	171/214(80%)		53/114(46%)
Prochlorococcus marinus str. MIT9123	258/337(77%)	171/214(80%)		53/114(46%)
Prochlorococcus marinus str. MIT9201	261/337(77%)	172/214(80%)		37/68(54%)
Prochlorococcus marinus str. MIT9202	262/337(77%)	148/186(80%)		37/68(54%)
Prochlorococcus marinus str. MIT9211	257/334(76%)	171/219(78%)		49/93(53%)
Prochlorococcus marinus str. MIT9215	262/337(77%)	171/214(79%)		37/68(54%)
Prochlorococcus marinus str. MIT9301	262/337(77%)	173/214(80%)		37/68(54%)
Prochlorococcus marinus str. MIT9302	262/337(78%)	173/214(81%)		38/79(48%)
Prochlorococcus marinus str. MIT9303	237/303(78%)	183/236(77%)		35/64(55%)
Prochlorococcus marinus str. MIT9311	260/337(77%)	174/214(81%)		37/67(55%)
Prochlorococcus marinus str. MIT9312	260/337(77%)	174/214(81%)		37/67(55%)
Prochlorococcus marinus str. MIT9313	265/337(78%)	178/218(81%)		37/67(55%)
Prochlorococcus marinus str. MIT9314	261/337(77%)	172/214(80%)		37/68(54%)
Prochlorococcus marinus str. MIT9322	262/337(78%)	173/214(81%)		37/68(54%)
Prochlorococcus marinus str. MIT9401	262/337(78%)	173/214(81%)		37/68(54%)
Prochlorococcus marinus str. MIT9515	263/337(78%)	169/214(79%)		32/59(54%)
Prochlorococcus marinus str. MIT0601	260/337(77%)	172/214(80%)		60/118(51%)
Prochlorococcus marinus str. MIT0604	262/337(78%)	172/214(80%)		37/68(54%)
Prochlorococcus marinus str. MIT0701	267/337(80%)	177/220(80%)		37/67(55%)
Prochlorococcus marinus str. MIT0702	268/337(80%)	177/220(80%)		37/67(55%)
Prochlorococcus marinus str. MIT0703	268/337(80%)	177/220(80%)		37/67(55%)
Prochlorococcus marinus str. MIT0801	259/334(78%)	174/222(78%)		38/68(56%)
Prochlorococcus marinus str. NATL1A	258/334(77%)	174/222(78%)		38/68(56%)
Prochlorococcus marinus str. NATL2A	257/334(76%)	174/222(78%)		38/68(56%)
Prochlorococcus marinus str. PAC1	257/334(77%)	174/222(78%)		38/68(56%)
Prochlorococcus marinus str. SB	260/337(77%)	173/214(81%)		37/68(54%)
Prochlorococcus marinus str. SS2	263/337(78%)	169/218(78%)		60/114(53%)
Prochlorococcus marinus str. SS35	263/337(78%)	169/218(78%)		60/114(53%)
Prochlorococcus marinus str. SS51	263/337(78%)	169/218(78%)		60/114(53%)
Prochlorococcus marinus str. SS52	263/337(78%)	169/218(78%)		60/114(53%)
Prochloron didemni			1831/2988(61%)	
Prochlorothrix hollandica	293/338(86%)	193/229(84%)		66/100(66%)
Pseudanabaena sp. PCC 7367	285/339(84%)	201/226(88%)		37/53(70%)
Raphidiopsis brookii D9	299/338(88%)	194/221(87%)		89/136(65%)
Rivularia sp. PCC 7116	294/338(86%)	194/228(85%)		73/110(66%)

Scytonema hofmanni UTEX B 1581	299/338(88%)	200/228(87%)		83/123(67%)
Scytonema millei	302/339(89%)	200/231(86%)		70/95(74%)
Scytonema tolypothrichoides	299/338(88%)	200/228(87%)		82/128(64%)
Stanieria cyanosphaera PCC7437			1899/2788(68%)	86/126(68%)
Synechococcus elongatus	279/337(82%)	195/231(84%)		78/118(66%)
Synechococcus sp. BL107	259/337(76%)	172/210(81%)		60/129(47%)
Synechococcus sp. CC9311	265/339(78%)	181/219(82%)		43/75(57%)
Synechococcus sp. CC9605	266/337(78%)	171/210(81%)		57/128(45%)
Synechococcus sp. CC9902	259/337(76%)	172/210(81%)		60/129(47%)
Synechococcus sp. NKBG15041c			2327/2724(85%)	93/135(69%)
Synechococcus sp. JA-2-3B'a(2-13)	268/338(79%)	179/221(80%)		33/64(52%)
Synechococcus sp. JA-3-3Ab	268/338(79%)	180/221(81%)		
Synechococcus sp. PCC6312	294/338(86%)	188/221(85%)		79/132(60%)
Synechococcus sp. PCC7002			2720/2720	90/133(68%)
Synechococcus sp. PCC7335	285/339(84%)	196/231(84%)		76/115(66%)
Synechococcus sp. PCC7502	283/339(83%)	188/222(84%)		80/139(58%)
Synechococcus sp. RCC307	265/337(78%)	182/220(82%)		59/130(45%)
Synechococcus sp. RS9916	263/337(78%)	173/210(82%)		38/69(55%)
Synechococcus sp. RS9917	262/337(77%)	176/210(83%)		53/116(46%)
Synechococcus sp. WH5701	264/334(79%)	182/220(82%)		42/67(63%)
Synechococcus sp. WH7803	264/337(78%)	180/219(82%)		42/75(56%)
Synechococcus sp. WH7805	265/337(78%)	175/210(83%)		51/103(50%)
Synechococcus sp. WH8102	263/337(78%)	174/210(82%)		60/128(47%)
Synechococcus sp. WH8109	265/337(78%)	174/210(82%)		44/94(47%)
Synechocystis sp. PCC6714	338/340(99%)	227/231(98%)		131/134(98%)
Synechocystis sp. PCC6803	340/340	231/231		149/149
Synechocystis sp. PCC7509	299/340(87%)	199/230(86%)		85/134(63%)
Thermosynechococcus elongatus BP-1	290/338(85%)	186/221(84%)		69/124(56%)
Tolypothrix campylonemoides	299/338(88%)	203/231(87%)		82/124(66%)
Tolypothrix sp. PCC7601	302/338(89%)	203/230(88%)		89/137(68%)
Trichodesmium erythraeum IMS101	297/338(87%)	192/220(87%)		66/93(71%)
Trichormus azollae	299/338(88%)	197/223(88%)		73/105(70%)
Xenococcus sp. PCC7305			1857/2848(65%)	87/137(64%)

Table S2: Cell size as determined via fluorescence microscopy. Values represent the cell diameter of *Synechocystis* cells and width/length of *Synechococcus* cells in μm. The cellular volume is measured in μm^3. Standard deviation (S.D.) is indicated. Asterisks indicate significant differences between samples (Student's t-test; P < 0.0001).

Strain	Cells counted	Cell size (Mean)	cell size (S.D.)	Cell volume (±S.D.)	Minimum cell size	Median cell size	Maximum cell size
Synechocystis							
Wild-type	171	2.06	0.13	4.63±0.83	1.60	2.08	2.38
ΔFAR	121	2.72*	0.34	11.02±4.23*	1.72	2.72*	3.85
ΔFAR:comp	186	2.09	0.15	4.83±0.99	1.60	2.08	2.40
Synechococcus							
Wild-type	102	1.61/2.30	0.13/0.50	3.08±0.72	1.36/1.60	1.58/2.21	2.13/4.36
Δols	128	1.76*/2.41	0.27/0.84	3.89±1.49*	1.36/1.40	1.7*/2.30	3.57/7.49

Table S3: Cell size as determined via particle counting measurements. Values represent the cell width/diameter of the cells in μm. The cellular volume is measured in μm^3. Standard deviation (S.D.) is indicated. Asterisks indicate significant differences between samples (P < 0.0001).

Strain	Cells counted	Cell size (Mean)	Cell size (S.D.)	Cell volume	Minimum cell size	Median cell size	Maximum cell size
Synechocystis							
Wild-type	1069396	2.06	0.31	4.58	1.60	2.08	2.38
ΔFAR	370156	2.80*	0.41	11.49*	1.72	2.72*	3.85
ΔFAR:comp	917114	2.00	0.23	4.19	1.60	2.08	2.40

Table S4: Cell counts of single and actively dividing *Synechocystis* cells. Asterisks indicate significant differences between samples (P < 0.05).

Strain	Single cells	Dividing cells	Total cells	% Single cells	% Dividing cells
Wild-type	257	172	429	59.9	40.1
ΔFAR	169	152	321	52.6*	47.4*
ΔFAR:comp	178	117	295	60.3	39.7

Table S5: Carotenoid/chlorophyll ratios in cyanobactrerial strains. Results are from three biological replicates.

Strain	Mean	S.D.
Synechocystis		
Wild-type	0.31369	0.10439
ΔFAR	0.39693	0.10933
ΔFAR:comp	0.42608	0.10330
Synechococcus		
Wild-type	0.91792	0.01904
ΔOls	1.28426	0.15799

Table S6: **Lipid composition of cyanobacterial membranes.** The experimental lipid composition according to Sheng *et al* is shown in mM, and has been adjusted to account for lipids rather than fatty acids. The simplified composition used in a 2,400 lipid bilayer in the *in silico* models is given in brackets. ND = not detected.

	PG	MGDG	SQDG	DGDG
2x16:0	0.041 (96)	0.329 (840)	0.239 (600)	0.082 (192)
16:0-16:1$^{\Delta 9}$	ND	0.044 (96)	0.040 (96)	0.006 (24)
16:0-18:1$^{\Delta 9}$	0.014 (48)	0.018 (48)	0.032 (96)	0.012 (48)
16:0-18:2$^{\Delta 9,12}$	0.006 (24)	0.030 (72)	0.017 (48)	0.010 (24)
16:0-α18:3$^{\Delta 9,12,15}$	ND	0.024 (48)	ND	ND
Total	**0.061 (168)**	**0.445 (1104)**	**0.328 (840)**	**0.110 (288)**

Table S7: Sequence of primers used in this study. Restriction endonuclease sites introduced into the primer are underlined.

Primer	Sequence
Sll0209for	GTAC<u>GCATGC</u>ACCTTGTTCACCAGCTCCAC
Sll0209rev	GTAC<u>TCTAGA</u>CAAAATGGAAAACCGCCATA
olsfor	GATC<u>GAATTC</u>AGCAAACCGTTTTTGTGACC
olsrev	GTAC<u>GTCGAC</u>TGCAAGGTGGCGAACTGTAT
phaABleftfor	GTAC<u>TCTAGA</u>GGGACCATCCTGACTACACG
phaABleftrev	GATC<u>GGATCC</u>GTTCGTTTAGCGGCAACAAT
phaABrightfor	GATC<u>GAGCTC</u>TTTTACTTTCCCCCGTAGCC
phaABrightrev	GACT<u>GAATTC</u>GCATTGTCTGGTCCATGTTG
Sll0209compfor	GATC<u>GGATCC</u>TTTGACCAGCAGCATTGAG
Sll0209comprev	GATC<u>GAGCTC</u>TTTCATGAGCCCACAAATCC
Phafor	ATTGTTGCCGCTAAACGAAC
Pharev	TACTGGCTACGGGGGAAAGT